Scaling relationships for event water contributions and transit times in small-forested catchments in Eastern Quebec

C. Segura,[1] A. L. James,[2] D. Lazzati,[3] and N. T. Roulet[4]

Received 20 January 2012; revised 3 May 2012; accepted 26 May 2012; published 4 July 2012.

[1] Recent studies of catchment hydrologic response are incorporating increasingly complex datasets to investigate model representation of spatial and temporal variability. In this paper, catchment rainfall-runoff and stable isotope tracer response were modeled using a lumped conceptual model that integrates the unit hydrograph and isotope hydrograph separation methodologies. The model was applied across eight nested catchments (7 to 147 ha) for four rainstorms collected between summer and fall in 2001–2002, generating a usable 23 rainstorm datasets ranging from 1.2 to 10.3 h in length and spanning variability in environmental conditions related to storm characteristics (size and intensity) and antecedent moisture. Monte Carlo simulations were run for four model structures of varying complexity and evaluated using a Generalized Likelihood Uncertainty Estimation (GLUE) approach. We found that a model of intermediate complexity was adequate to model all catchment-storm pairs. Relationships between the parameters of the best model and catchment and storm characteristics were sought. We found that the fraction of effective rainfall routed as event water was correlated to rainstorm size but insensitive to catchment size, indicating that it is controlled by environmental conditions such as storm intensity and size. The mean transit time of event water decreased with increasing rainstorm size, indicating increased connectivity during larger rainstorms. Finally, a linear relation was found between the mean transit time of event water and catchment size suggesting that the time it takes for event water to be transferred to the stream is directly related to catchment size, particularly for catchments greater than 30 ha.

Citation: Segura, C., A. L. James, D. Lazzati, and N. T. Roulet (2012), Scaling relationships for event water contributions and transit times in small-forested catchments in Eastern Quebec, *Water Resour. Res.*, *48*, W07502, doi:10.1029/2012WR011890.

1. Introduction

[2] Comprehensive understanding of streamflow generation processes, their temporal variability and their spatial heterogeneity continues to offer contemporary challenges to practicing and research hydrologists [*Kirchner*, 2006; *McDonnell et al.*, 2007]. Recent investigations have tackled these challenges from both empirical and modeling approaches. Empirical approaches incorporating hydrometric, geochemical, and/or isotopic concentration data have attempted to achieve hydrologic understanding of the influence of geology, topography, antecedent moisture conditions (AMC), and catchment size on the rainfall-runoff process through observations made at specific catchments [*Mulholland et al.*, 1990; *Sklash*, 1990; *Sidle et al.*, 1995; *Brown et al.*, 1999; *Shanley et al.*, 2002; *McGlynn et al.*, 2004; *Onda et al.*, 2006]. The use of stable isotopes in investigations of streamflow generation continues to expand across varied landscapes and land-use [e.g., *Kabeya et al.*, 2007; *Jeelani et al.*, 2010; *Moravec et al.*, 2010; *Liu et al.*, 2011]. On the modeling side, *Beven* [2001, 2009] and *Wagener et al.* [2004] offer recent reviews of rainfall-runoff modeling, providing new frameworks and toolboxes for improved treatment of uncertainties due to both model structure and parameters. Many modeling efforts that incorporate environmental tracer data have considered a single catchment and a single set of conditions [*Seibert et al.*, 2003; *Soulsby and Dunn*, 2003; *Weiler et al.*, 2003; *Iorgulescu et al.*, 2005; *Lyon et al.*, 2008]. Despite the combined effort, it is still immensely challenging to predict behavior in regions lacking data or outside the range of observed or modeled conditions. In light of these difficulties emphasis has recently been placed on studies that incorporate both the experimental (i.e., data based) and conceptual modeling (i.e., based on conceptual representations of the processes) viewpoints [e.g., *Seibert and McDonnell*, 2002; *Iorgulescu et al.*, 2007; *Son and Sivapalan*, 2007; *Tetzlaff et al.*, 2008]. Even though several of these new frameworks have provided a more realistic representation of the runoff generation process, there continues to be a need for datasets and modeling efforts that examine spatial and temporal variability of response to try to understand the physical development of the rainfall-runoff process in terms of its

[1]Department of Forestry and Environmental Resources, North Carolina State University, Raleigh, North Carolina, USA.
[2]Department of Geography, Nipissing University, North Bay, Ontario, Canada.
[3]Department of Physics, North Carolina State University, Raleigh, North Carolina, USA.
[4]Department of Geography, McGill University, Montreal, Quebec, Canada.

Corresponding author: C. Segura, Department of Forestry and Environmental Resources, North Carolina State University, Raleigh, NC 27695, USA. (csegura@ncsu.edu)

0043-1397/12/2012WR011890

aggregation in space (e.g., as drainage area changes) and time (e.g., as the size of the storm changes) [*Kirchner*, 2006; *McDonnell et al.*, 2007]. This understanding would eventually allow transferring results between geographic regions and ultimately enable the prediction of the runoff response in ungauged catchments.

[3] Over the last decade emphasis has shifted from using hydrologic models to reproduce and predict streamflow toward the use of modeling as a learning tool to understand hydrologic behavior and its physical foundations [*Fenicia et al.*, 2008; *Bai et al.*, 2009; *Birkel et al.*, 2010]. Recently, such efforts have emphasized the importance of incorporating auxiliary data in addition to streamflow to improve catchment representation, the definition of model structure, and to aid in model evaluation by constraining model parameters. Auxiliary data incorporated in modeling studies to aid calibration include soil properties [e.g., *Atkinson et al.*, 2002; *Eder et al.*, 2003; *Farmer et al.*, 2003], the distribution of saturated areas [e.g., *Franks et al.*, 1998; *Guntner et al.*, 1999], environmental tracer response [e.g., *Seibert and McDonnell*, 2002; *Weiler et al.*, 2003; *Iorgulescu et al.*, 2005; *Tetzlaff et al.*, 2008], and groundwater levels [e.g., *Lamb et al.*, 1997; *Freer et al.*, 2004; *Fenicia et al.*, 2008].

[4] Relevant to the purpose of this study are conceptual modeling efforts that incorporate stable isotope ($\delta^{18}O$, δD) tracer data in model formulation and evaluation. These studies range in temporal scale, from multiannual analysis of mean residence time [see *McGuire and McDonnell*, 2006] to seasonal time-scale studies [e.g., *Seibert and McDonnell*, 2002; *Soulsby and Dunn*, 2003; *Iorgulescu et al.*, 2005, 2007; *Fenicia et al.*, 2008; *Birkel et al.*, 2010], to event-based studies [e.g., *Weiler et al.*, 2003; *Johnson et al.*, 2007; *Lyon et al.*, 2008; *Tetzlaff et al.*, 2008; *Roa-Garcia and Weiler*, 2010]. The spatial scale within this last group of studies currently varies between 2 and 3100 ha. For example, *Seibert and McDonnell* [2002] used estimates of new water contributions derived from isotope hydrograph separation in a short-term (1 month) lumped reservoir model of the 17 ha Maimai catchment; new water contributions based on $\delta^{18}O$ observations from six rainstorms were used to calculate the degree of acceptance of model runs. They found that the incorporation of these auxiliary data resulted in lower overall model efficiency (i.e., lower value of the objective function) but overall improved model performance (i.e., better agreement between new water contributions estimated by the model versus experimental observations). Modeling the same Maimai catchment data set, *Fenicia et al.* [2008] derived a series of conceptual semidistributed models. They showed that the level of complexity of the model had to increase as additional data was progressively incorporated into the model structure. Their final model structure was able to better capture the hydrologic response of the catchment by the incorporation of both stable isotope data and groundwater level observations.

[5] End-member-mixing-analyses have also been incorporated in conceptual modeling. The results from a three end-member analysis conducted in a 1000 ha Scottish catchment were used to validate the outcome of the conceptual semidistributed model DIY [*Soulsby and Dunn*, 2003]. A study conducted in a small Swiss catchment (20 ha) used the results from end-member-mixing-analysis together with streamflow observations [*Iorgulescu et al.*, 2005]. The use of both tracers and streamflow improved the constraints on the parameter space and required an increase in model complexity, revealing the existence of an interflow component.

[6] At the event time-scale, most conceptual model studies incorporating tracer data have been based on the "transfer function hydrograph separation" (TRANSEP) framework proposed by *Weiler et al.* [2003]. This framework integrates the unit hydrograph and the isotope hydrograph separation (IHS) techniques in a quantitative approach that allows the analysis of the temporal variability of streamflow partitioned into event and preevent components. The framework was conceived to provide an alternative approach to hydrograph separation based on a variety of tracers such as $\delta^{18}O$ [*Weiler et al.*, 2003; *Lyon et al.*, 2008] and CO_2 [*Johnson et al.*, 2007].

[7] The necessity to increase the complexity of the conceptual model whenever new data are added exemplifies our lack of understanding of the physical processes involved in runoff generation and the need of further theoretical and experimental investigations. The ultimate goal is to derive models with predictive power, i.e., capable of reproducing a data set over which they had not been previously calibrated [*Pomeroy et al.*, 2007]. An interesting direction along with these studies is that of modeling hydrologic response from different catchments of different size and physiographic and climatic characteristics, under different environmental conditions (e.g., antecedent moisture conditions, rainstorm size). *Weiler et al.* [2003] suggest that one of the values of the TRANSEP model is its potential as a tool to examine scaling behavior of the transit time of water in a very efficient way. Such efforts would allow the study of the model parameters across catchment characteristics and environmental conditions, lending insight in the underlying physical processes. These studies would also guide the development of a model parameterized on easily measured characteristics (e.g., catchment size, dominant soil type, surface or subsurface topography) or conditions (rainstorm size and intensity and antecedent moisture conditions) rather than on internal model parameters such as mean transit times or water routing parameters. A recent study combining hydrometric and stable isotope tracer data together with transit times computed using the TRANSEP model for a series of 18 storms in the Cascades (OR) found that both hillslope and catchment streamflow responded almost linearly with storm size when antecedent rainfall was above 20 mm [*McGuire and McDonnell*, 2010].

[8] In this paper, we use a data set of streamflow and $\delta^{18}O$ collected from eight nested catchments with variable catchment area (7 to 147 ha) within the forested Mont Saint–Hilaire UNESCO Biosphere reserve to explore the spatial and temporal dependence of catchment response using a conceptual model based on the TRANSEP model of *Weiler et al.* [2003]. The aim is to investigate general behavior of event time-scale catchment response [*McDonnell et al.*, 2007] through the comparison of model catchment parameters over space and time. IHS has already been performed on this data set [*James and Roulet*, 2009]. The specific objectives of this study are (1) to develop a TRANSEP-inspired model [*Weiler et al.*, 2003] with different degrees of complexity integrating the instantaneous unit hydrograph and the IHS rainfall-runoff and isotope tracer

response, (2) to apply the model to the Mont-Saint-Hilaire data set (four rainfall-runoff periods observed across 8 nested catchments), (3) to evaluate the required level of model complexity and behavioral range of parameters across the nested catchments and varying environmental conditions (antecedent moisture conditions, storm characteristics) and (4) to use the spatial and temporal variability of parameterization to investigate the behavior of hydrologic response with respect to catchment and rainstorm characteristics and to explore the possibility of predicting model parameters based on such easily measurable characteristics.

2. Study Site

[9] This study was conducted in the Westcreek watershed of the Mont Saint Hilaire UNESCO Biosphere reserve, southern Quebec, Canada. The watershed is covered by old-growth deciduous forest dominated by Sugar maple (*Acer saccharum*) and American beech (*Fagus grandifolia*). Rainfall averages ~80 mm month^{-1}, with a mean annual of 940 mm, 78% received as rain and 22% as snow. Mean daily temperature has strong seasonality, varying between −10.3°C in winter and 20.8°C in summer. The largest, third-order catchment (LK) drains 147 ha over 237 m of relief. The remaining seven, nested catchments of orders 1 to ~2 range in size between 7 and 91 ha (Figure 1 and Table 1). Five of the catchments are perennial and three are ephemeral with flow absent part of the ice-free period. Average catchment slope varies between 13.5 and 23.1% and valley-bottom area (defined by a break in slope of 8°) varies between 1.2 and 38.7 ha [*James and Roulet*, 2009]. Data on soil depth is limited to select areas (e.g., AW and VC catchments). On the hillslopes, soils are well drained with typical depths between 0 (outcrop) to 1.5 m, whereas in the valley bottoms they can be >2 m; here, the presence of a low-permeability layer or fragipan [*Dingman*, 1994] within 30–50 cm of the surface can generate perched water tables that intermittently connect to stream channels [*James and Roulet*, 2006]. The presence

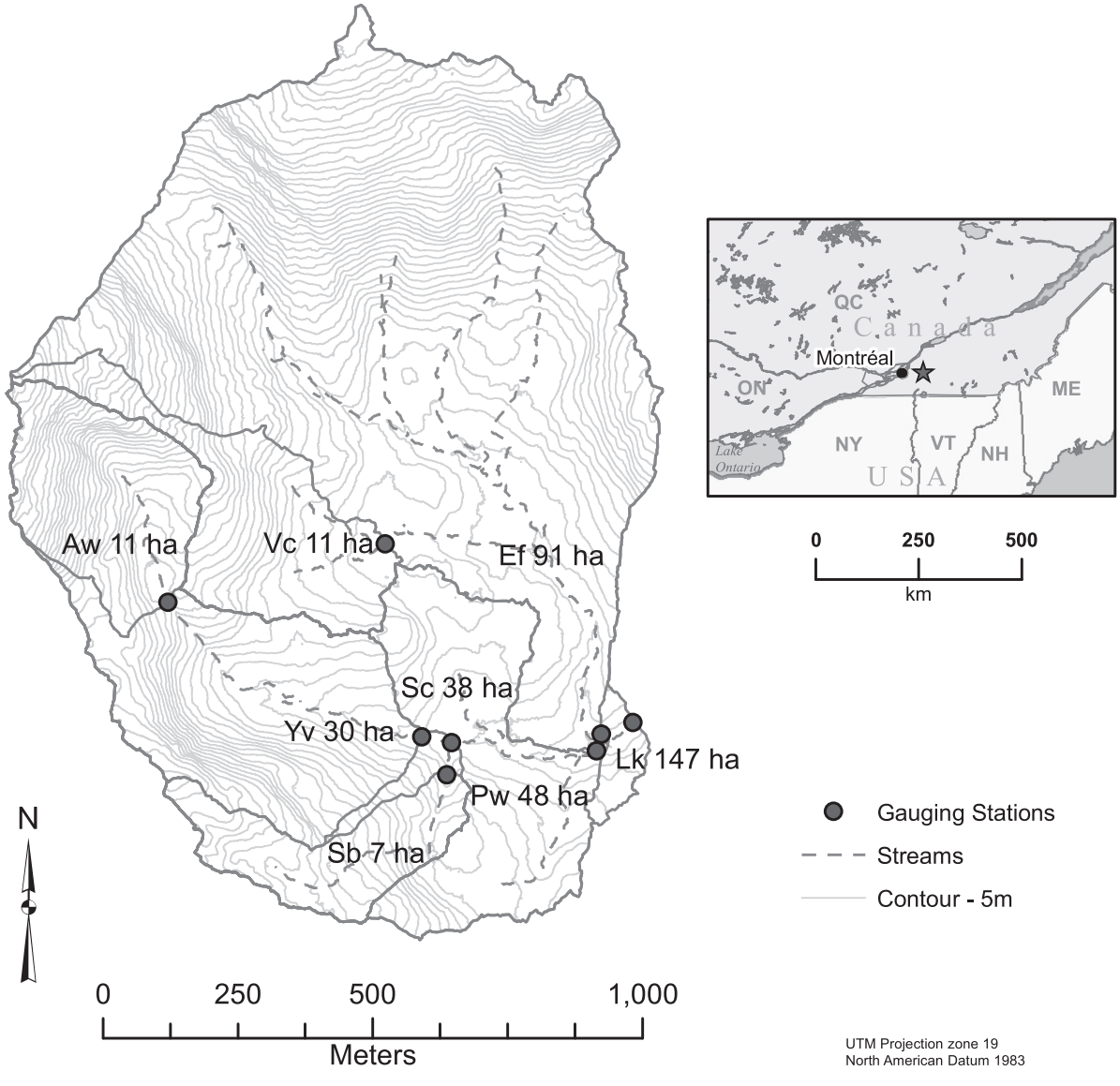

Figure 1. Westcreek watershed, Mont Saint-Hilaire, Quebec, Canada. Eight small nested catchments are defined.

Table 1. Storm Characteristics and Number of Measurements of Streamflow Q and $\delta^{18}O$ Composition Available Per Catchment-Rainstorm Pair[a]

Catchment Name, Status, (Order)	Catchment Area (ha)	Storm 8[b]	Storm 10[c]	Storm 11[d]	Storm 1[e]
LK, perennial (3)	147	81 (10)	250 (10)	9 (9)[f]	73 (9)
EF, perennial, (~2)	91	70 (11)	7 (8)[f]	9 (8)[f]	N/A[g]
PW, perennial, (2)	48	77 (10)	9 (9)[f]	9 (9)[f]	N/A
SC, perennial, (2)	38	77 (10)	99 (8)	6 (7)[f]	70 (10)
YV, ephemeral, (1)	30	9 (9)[f]	N/A	dry	68 (7)
VC, ephemeral, (1)	11	11 (10)[f]	99 (9)	dry	N/A
AW, perennial, (1)	11	11 (11)[f]	11 (11)[f]	8 (8)[f]	24 (14)
SB, ephemeral, (1)	7	120 (11)	N/A	dry	dry

[a]API is antecedent rainfall over the previous 7, 14, and 25 days in mm, average (AI) and maximum (Max.int) rainfall intensities are given in mm/15 min. $\delta^{18}O$ composition is in parentheses.
[b]Size = 14.1 mm; $API_7 = 15.1$; $API_{14} = 85.1$; $API_{25} = 150$; Duration = 1.2 h; AI = 2; Max.int = 6.6.
[c]Size = 38.1 mm; $API_7 = 4.8$; $API_{14} = 24.4$; $API_{25} = 27.0$; Duration: 2.4 h; AI = 3.8; Max.int = 6.3.
[d]Size = 7 mm; $API_7 = 0$; $API_{14} = 0$; $API_{25} = 7.8$; Duration: 2.9 h; AI= 0.6; Max.int = 2.6.
[e]Size = 25.2 mm; $API_7 = 1.1$; $API_{14} = 1.1$; API_{25} =N/A; Duration: 10.3 h; AI = 0.6; Max.int = 12.2.
[f]Only manual stage measurements were available.
[g]N/A: Indicates not available.

of pockets of glacial till may also offer variation in soils and subsurface storage that are not necessarily identifiable from DEM-derived characteristics. A full description of the study area, including additional details on individual catchment characteristics can be found in previous publications [*James and Roulet*, 2006, 2007, 2009].

3. Methods

3.1. Hydrometric and Stable Isotope Tracer Data

[10] Rainfall-runoff and stable isotope data collected during the summer of 2001–2002 are available for five rainstorms [see also *James and Roulet*, 2009], four of which are used for modeling in this study (Table 1). The four rainstorms occurred under intermediate-wet to dry conditions and vary in magnitude from 7 to 38 mm. Antecedent rainfall over the previous 7 (API_7), 14 (API_{14}), and 25 (API_{25}) days range between 0–65 mm, 0–85 mm, and 7.8–150 mm, respectively (Table 1). Based on the antecedent precipitation data mentioned storms 1, 10, and 11 occurred under relatively dry conditions, whereas storm 8 occurred under relatively wet conditions [*James and Roulet*, 2009]. Throughfall was recorded at 15 min resolution at on-site tipping bucket gauges located at the highest elevation, most upstream (AW) and lowest elevation, most downstream (LK) gauging stations and were verified against bulk manual measurements. Throughfall sampling for isotope compositions did not include sequential sampling. Table 1 shows the total number of measurements of streamflow (stage) and streamflow samples (isotope compositions) per catchment-rainstorm pair. Streamflow stage was recorded electronically with potentiometers or pressure transducers (every 15 min) at the eight catchments gauging stations. In some instances electronic measurements failed and manual stage data collected simultaneously with stream water isotope sampling during the rainstorms were used instead. Streamflow was unavailable for five catchment-rainstorm pairs (Table 1, N/A). During two rainstorms no streamflow (Table 1, dry) was generated in a number of the ephemeral catchments (e.g., YV, VC, and SB), leaving a total of 23 catchment-rainstorm pairs for modeling purposes.

[11] All throughfall and streamflow (base flow and stormflow) samples were analyzed for $\delta^{18}O$ by the University of Waterloo's Environmental Isotope Laboratory. Blind samples provided a mean repeatability of $\delta^{18}O$ compositions of $\pm 0.09‰$. The $\delta^{18}O$ composition of new or event-water (C_e) delivered during each storm was calculated from the volume weighted average of throughfall compositions collected at 15 manual collectors; information on intrastorm variability was not collected. Standard deviation in event-water composition due to spatial variability was below 0.16‰ for all storms except for rainstorm 11 where the standard deviation was 0.42‰. Old or preevent-water $\delta^{18}O$ compositions (C_p) were defined by base flow collected at each gauging station prior to each storm event. Spatial variability in preevent water composition was within 0.25‰. Uncertainty in instantaneous streamflow was estimated as ± 1 standard deviation of the best-fit rating curve coefficients for each gauging station. This resulted in uncertainties expressed as a percentage of streamflow that varied between 9.7% and 30% with a mean of 16% [*James and Roulet*, 2009].

3.2. Model Description

[12] We use a model structure inspired by TRANSEP [*Weiler et al.*, 2003] which integrates the unit hydrograph approach [*Sherman*, 1932] with IHS [*Sklash and Farvolden*, 1979]. The schematic of the model used here is illustrated in Figure 2. The model is based on the assumption that rainfall-runoff can be partitioned between event and preevent components. Event-water corresponds to streamflow generated directly from water delivered during the rainstorm and preevent water corresponds to streamflow generated from water stored in the catchment before the rainstorm event. Similar to many rainfall-runoff models [e.g., IHACRES, *Jakeman et al.*, 1990] our model has a nonlinear module that transforms precipitation or throughfall into effective rainfall [*Jakeman and Hornberger*, 1993]. The effective rainfall is then partitioned into event and preevent water and convolved with a transfer function to produce rainfall-induced runoff (i.e., excluding base flow) from both event and preevent water contributions. The sum of these two components gives the total runoff. The model structure can accommodate different choices for the partition of the effective rainfall into event and preevent components and for the complexity of the transfer functions. In this work, we

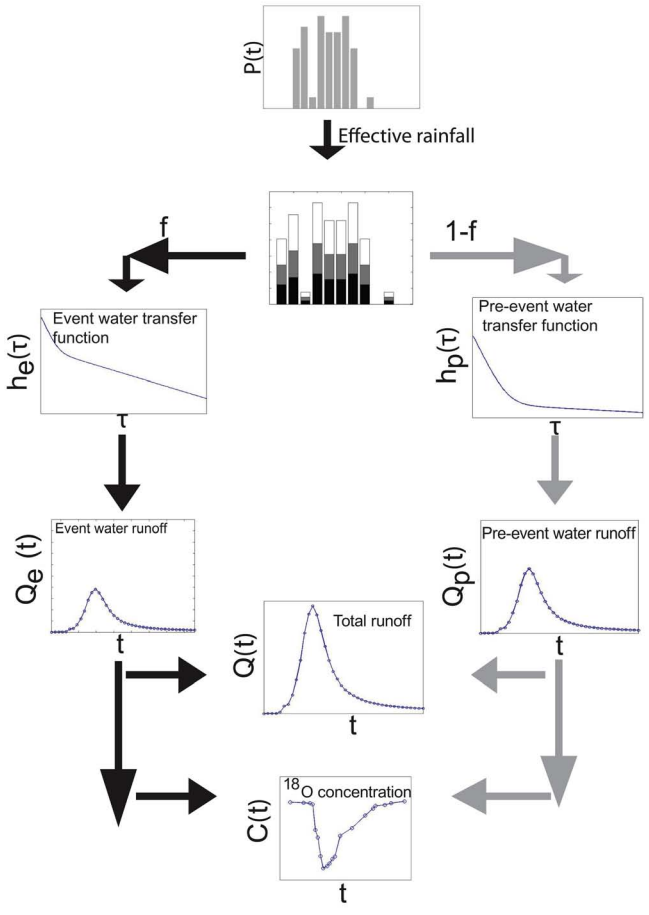

Figure 2. Schematic representation of the general model structure inspired by TRANSEP [*Weiler et al.*, 2003]. All parameters are fitted simultaneously. Difference in four different model structures are described in Table 2.

explore two schemes for the effective rainfall partition and two families of transfer functions for event and preevent water contributions, for a total of four different models. In two of the models, the fraction f of effective rainfall routed as event water is held constant throughout the storm, while in the other two models f is allowed to vary with the storm intensity, following *Weiler et al.* [2003]. Two of the models adopt a linear reservoir transfer function for each event and preevent, while the other two consider two linear parallel reservoirs. The details of the four model structures considered here are described below and reported in Table 2.

3.2.1. Module 1: Effective Rainfall

[13] The first module of the model is a nonlinear routine that computes the effective rainfall (P_{eff}) as the product of rainfall and the antecedent rainfall index $s(t)$ [*Jakeman and Hornberger*, 1993]:

$$P_{eff}(t) = p(t)s(t), \tag{1}$$

where $s(t)$ is computed by exponentially weighting rainfall p backward in time with a memory timescale parameter w, through the equation [*Weiler et al.*, 2003]:

$$s(t) = cp(t) - s(t - \Delta t)\left(1 - \frac{1}{w}\right), \tag{2}$$

where c is a normalization constant that is calculated a posteriori from the hydrometric data to maintain the water balance ($\Sigma P_{eff} = \Sigma Q$). The initial value of s, indicated as s_0, and the time constant w are the two free parameters of this module.

3.2.2. Module 2: Event and Preevent Routing

[14] Effective rainfall (P_{eff}) is routed as either event or preevent water. A fraction $f < 1$ of the effective rainfall is

Table 2. Model Structure, Parameters Per Module, Initial Parameter Ranges, and Total Number of Parameters Per Model Structure[a]

Parameter	Units	Model 1	Model 2	Model 3	Model 4
			Effective Rainfall		
s_0	–	0–1	0–1	0–1	0–1
w	15-min time steps	0–40	0–40	0–40	0–40
			f		
c_f	15-min mm^{-1}	–	0–1	–	0–1
w_f	15-min time steps	–	0–40	–	0–40
f	–	0–1	–	0–1	–
			Reservoirs of Event and Preevent Water		
q_e	–	–	–	0–1	0–1
$\boldsymbol{k_e}$	h	**0–50**	**0–50**	–	–
$\boldsymbol{k_{fe}}$	h	–	–	**0–50**	**0–50**
k_{se}	h	–	–	0–125	0–125
q_p	–	–	–	0–1	0–1
$\boldsymbol{k_p}$	h	**0–125**	**0–125**	**–**	**–**
$\boldsymbol{k_{fp}}$	h	**–**	**–**	**0–50**	**0–50**
k_{sp}	h	–	–	0–125	0–125
			Equations (See Section 3.2. Model Description)		
		1, 2, 4, 5, 7, 9, 10, 11	1, 2, 3, 4, 5, 7, 9, 10, 11	1, 2, 4,6, 8, 9, 10, 11	1, 2, 3, 4, 6, 8, 9, 10,11
			Total Number of Parameters		
		5	6	9	10

[a]In bold are parameters for which initial ranges were progressively narrowed.

routed as event water; while the remaining fraction $(1 - f)$ is routed as preevent water. Since hydrograph separation studies have found that f depends on total rainfall amount, rainfall intensity, and antecedent wetness conditions [*Bottomley et al.*, 1984; *McDonnell et al.*, 1990; *Pionke and Dewalle*, 1992], *Weiler et al.* [2003] suggested the use of a time-variable f through the rainstorm, parameterized with an equation analogous to equation (2) in which $s(t)$ is replaced with $f(t)$ and $f(0) = 0$:

$$f(t) = c_f p(t) - f(t - \Delta t)\left(1 - \frac{1}{w_f}\right). \tag{3}$$

[15] In this study we explored both the possibility of a constant f (models 1 and 3) and the possibility of a variable f as given by equation (3) (models 2 and 4). This module has a single free parameter (f) in models 1 and 3 and has two free parameters (c_f and w_f) in models 2 and 4 (Table 2).

3.2.3. Module 3: Event and Preevent Transfer Functions

[16] The fraction f of effective rainfall routed as event water is convolved with a transfer function, $h_e(\tau)$ to find the event water runoff:

$$Q_e(t) = \int_0^t h_e(\tau) P_{eff}(t - \tau) f(t - \tau) d\tau. \tag{4}$$

Two different transfer functions were explored: the first describes a single linear reservoir:

$$h_e(\tau) = \frac{1}{k_e} \exp\left(-\frac{\tau}{k_e}\right), \tag{5}$$

where k_e is the mean transit time; the second describes two linear reservoirs in parallel:

$$h_e(\tau) = \frac{q_e}{k_{fe}} \exp\left(-\frac{\tau}{k_{fe}}\right) + \frac{1 - q_e}{k_{se}} \exp\left(-\frac{\tau}{k_{se}}\right), \tag{6}$$

where q_e is the fraction of water routed into the fast-responding reservoir and k_{fe} and k_{se} are the mean transit times of the fast and slow reservoirs, respectively. These transfer functions were suggested by *Weiler et al.* [2003] in the TRANSEP formulation and have been successful at modeling rainfall-runoff response in a number of situations [*Weiler et al.*, 2003; *Iorgulescu et al.*, 2005; *Johnson et al.*, 2007; *Lyon et al.*, 2008; *Birkel et al.*, 2010; *Roa-Garcia and Weiler*, 2010].

[17] Two analogous transfer functions were used to describe the generation of the preevent runoff:

$$h_p(\tau) = \frac{1}{k_p} \exp\left(-\frac{\tau}{k_p}\right) \tag{7}$$

and

$$h_p(\tau) = \frac{q_p}{k_{fp}} \exp\left(-\frac{\tau}{k_{fp}}\right) + \frac{1 - q_p}{k_{sp}} \exp\left(-\frac{\tau}{k_{sp}}\right), \tag{8}$$

with the symbols having the same meaning as for equations (5) and (6) but for the preevent water. In all cases the time constants of the event and preevent water transfer functions were left free to vary independently in order to take into account the fact that the speeds of propagation of the pressure wave (hydraulic response) and solute transport (isotopes) are different [*Weiler et al.*, 2003]. An analogous convolution was also used to calculate the preevent runoff:

$$Q_p(t) = \int_0^t h_p(\tau) P_{eff}(t - \tau) f(t - \tau) d\tau. \tag{9}$$

[18] Once the event (Q_e) and preevent (Q_p) runoff have been computed, the tracer composition (e.g., $\delta^{18}O$) in the stream is calculated as:

$$c(t) = \frac{Q_e(t) C_e + \lfloor Q_p(t) + Q_b \rfloor C_p}{Q_e + Q_p + Q_b}, \tag{10}$$

where C_e is the tracer composition of event water (rainfall), C_p is the tracer composition in preevent water (e.g., base flow prior to the rainstorm), and Q_b is base flow streamflow. In this study, due to the absence of data on the variability of C_e during a rainstorm (i.e., sequential sampling of rainfall), the model assumes that C_p and C_e are constant over the duration of the rainstorm. This assumption is a potential shortcoming of the data set that could have identified an additional source of experimental uncertainty that will potentially limit model structure evaluation. Conversely, the original version of TRANSEP *Weiler et al.* [2003] allows for C_e to vary over the duration of the storm.

[19] Once the best-fit transfer functions for event and preevent water have been found by data-fitting, total runoff can be calculated as the sum of event and preevent water. The total water transfer function $g(\tau)$ can be obtained through the implicit equation:

$$\int_0^t g(\tau) P_{eff}(t - \tau) d\tau = \int_0^t h_e(\tau) P_{eff}(t - \tau) f(t - \tau) d\tau + \int_0^t h_p(\tau) P_{eff}(t - \tau)[1 - f(t - \tau)] d\tau. \tag{11}$$

Practically, computing $g(\tau)$ would require a deconvolution, an operation that even numerically is fraught with severe instabilities. The main difference between TRANSEP [*Weiler et al.*, 2003] and our modeling approach is that we focus on the transfer functions of event and preevent water (i.e., pulling out parameters for $h_e(\tau)$ and $h_p(\tau)$), fitting them directly and simultaneously using the measurements of total streamflow and isotope concentrations). In contrast, TRANSEP focuses on the transfer functions of total streamflow ($g(\tau)$) and of solute (isotopes concentrations), and fits them in sequence.

[20] Table 2 summarizes the four model structures considered and the free parameters relevant to each of the models. Model 1 has a constant fraction of effective rainfall routed as event water (f) and a single reservoir for each event and preevent water; model 2 has time-variable f and a single reservoir for each event and preevent water; model 3 has constant f and two reservoirs in parallel for both event and preevent water, and model 4 has time-variable f and

two reservoirs in parallel for each event and preevent water. For all four models, streamflow (Q) and isotopic concentrations ($\delta^{18}O$) are computed every 15 min. For rainstorms with limited streamflow data, model predictions were interpolated to match the time series of the observations (Q and $\delta^{18}O$). The total number of parameters for the four model structures varies between 5 and 10 (Table 2).

3.3. Model Parameterization and Performance

[21] Our initial intent was to model each catchment-rainstorm pair using the four model structures described above. However, based on early simulation results for a subset of 13 catchment-rainstorm pairs spanning the range of catchment sizes and storms, this strategy was modified, (see section 4.1), and only one of the four model structures was considered for modeling of the remaining 10 catchment-rainstorm pairs. The decision of abandoning three of the models was based both on comparisons of model performance measured with the Nash Sutcliffe (NS) efficiency coefficient [*Nash and Sutcliffe*, 1970] and the level of model parsimoniousness measured with the Akaike Information Criterion (AIC) [*Akaike*, 1974]. The AIC provides a quantitative tool with which to distinguish the most parsimonious model among several. It is defined as:

$$AIC = -2\log(m) - 2k, \tag{12}$$

where m is the maximum likelihood and k is the number of parameters in the model. The χ^2 statistic was used as the likelihood since $-2\log(m) = \chi^2$ [*Bevington and Robinson*, 2003] and

$$\chi^2 = \sum_{i=1}^{N} \frac{(O_i - P_i)^2}{\sigma_i^2}, \tag{13}$$

where O_i and P_i are observed and predicted values of streamflow or $\delta^{18}O$ composition and σ_i is the uncertainty associated with the observed values. As mentioned in section 3.1 streamflow uncertainties varied between 9.7 and 30.4% and $\delta^{18}O$ uncertainties between 0.16 and 0.42‰. The sum of the AIC for streamflow and $\delta^{18}O$ was calculated for each of the initial 13 catchment-rainstorm pairs and then ranked. The model with the lowest AIC is the most efficient at fitting the observed values. The AIC not only rewards goodness of fit, but also penalizes models with higher number of parameters providing a measure of parsimoniousness. Results were confirmed by visual inspection of the observed and predicted time series of runoff and $\delta^{18}O$ composition. The model parameterization and performance was separated into two steps:

3.3.1. Initial Simulation of 13 Storms Using Four Model Structures

[22] A Monte Carlo approach was used to generate random parameter sets for which total streamflow (Q) and tracer composition ($\delta^{18}O$) were simulated. For each of the 13 catchment-rainstorm pairs, an initial run of 10 million simulations was performed for each of the four models with the widest parameter ranges; some parameter ranges were then progressively narrowed over 1 to 4 sets of runs (see Table 2 for initial parameter ranges). This narrowing was only performed for some of the well-identified parameters and was done with care so that all the parameter space of behavioral simulations was sampled. At this time, the level of identification of the parameters was assessed by visual analysis of dotty plots. For example, Figure 3 illustrates the model 1 simulation results for catchment-pair EF-8. In Figure 3, parameters f, and time constants k_e, and k_p are well identified. The only parameters for which the initial

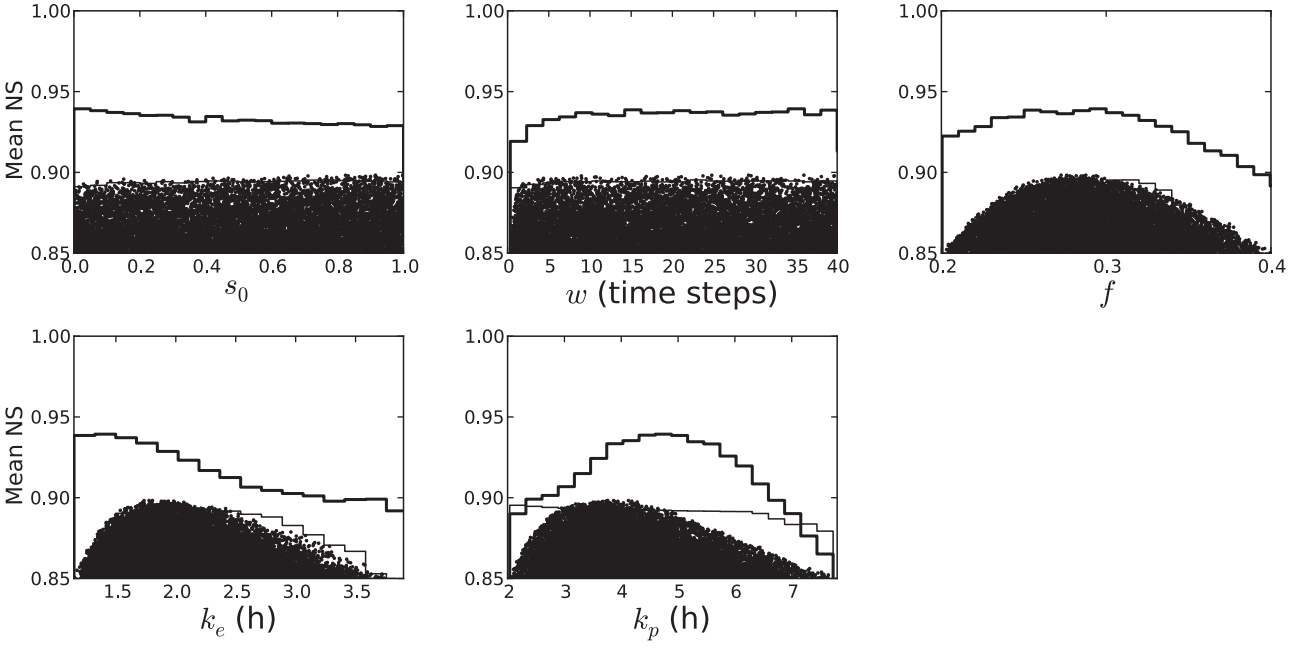

Figure 3. Dotty plots of model 1 parameters for catchment-storm pair EF-8. Note that the y axis starts at the behavioral threshold (mean NS = 0.85); there are 11,636 behavioral runs. The thick line represents the maximum NS for streamflow (Q) alone and the lighter line the maximum NS for $\delta^{18}O$ alone. Each dot represents the mean NS (Q and $\delta^{18}O$) for one behavioral run.

parameter space was reduced were the time constants k_e and k_p, for Models 1 and 2 and k_{fe} and k_{fp} for Models 3 and 4 (Table 2). We ran a minimum of 20 million simulations per model and catchment-storm pair and a maximum of 200 million simulations. In order to ensure that the number of simulations was large enough to capture the best efficiency the following procedure was followed: We performed a set of runs with increasing number of simulations where run i contained a total number of simulations proportional to 2^i. We then let i grow until the standard deviation of the efficiencies found in the last 4 runs was less than 1% of their average. We then retained the last run, with the highest number of simulations, as the final set of simulations with which to compare results of the 4 models. This scheme ensured that no additional simulations would have resulted in a significant improvement of model performance, in other words, that each model structure was fully evaluated. All parameters for each model structure were fit simultaneously. Model performance was evaluated using the Nash Sutcliffe (NS) efficiency coefficient [*Nash and Sutcliffe*, 1970] for both streamflow and $\delta^{18}O$ compositions. We selected an arbitrary NS threshold of 0.85 to classify evaluated parameter sets as "behavioral" or "nonbehavioral." Recent studies have used NS values ranging from 0.15 to 0.85 to define behavioral versus nonbehavioral simulations [e.g., *Iorgulescu et al.*, 2005; *Son and Sivapalan*, 2007; *Fenicia et al.*, 2008; *Hrachowitz et al.*, 2009; *Salazar et al.*, 2010].

[23] We gave equal importance to the fit of streamflow and $\delta^{18}O$; a "behavioral" set required a NS $\geq$ 0.85 for both streamflow and $\delta^{18}O$ compositions. A similar approach was taken by *Iorgulescu et al.* [2005] who also used NS for streamflow and silica and calcium tracer compositions. Other objective functions have been used to evaluate the performance of tracer compositions (e.g., the root-mean-square error, *Weiler et al.* [2003]) however NS was selected here because it is dimensionless. Once the best parameter set for each model was found, both the NS efficiency and the AIC were used to select the best model structure, in terms of both strength of the fit and parsimoniousness.

3.3.2. Simulation of All Catchment-Storm Pairs Using Model 3

[24] Based on the results attained in step 1 for 13 catchment-storm pairs only model 3 was used to simulate the remaining 10 catchment-storm pairs. The total number of model 3 simulations performed for each of the 23 catchment-storm pairs was a function of two criteria (1) the criteria implemented in the previous step (i.e., a the standard deviation of the efficiencies found in the last 4 runs less than 1% of their average) and (2) a minimum of 1000 behavioral parameter sets in order to apply the GLUE methodology. As a result, the total number of simulations performed for model 3 varied between 20 and 27,000 million runs (Figure 4).

3.4. Model 3 Parameter Identification

[25] A preliminary estimate of the level of identification of model 3 parameters was achieved by visual inspection of dotty plots. In addition, a measure of identification (MI) of

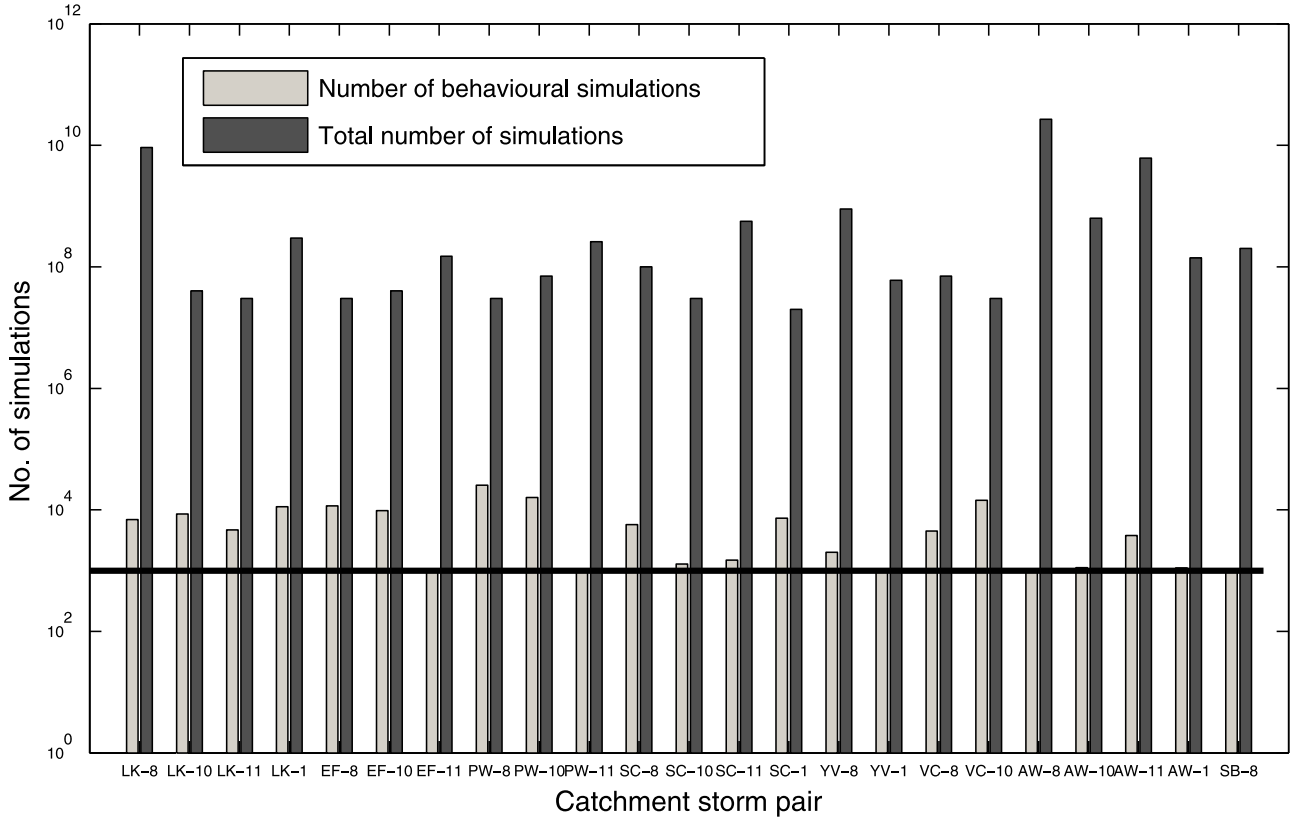

Figure 4. Total number of model 3 simulations performed for each catchment-storm pair and number of behavioral parameter sets. The minimum number of 1000 behavioral simulations considered to fully apply GLUE is displayed as a solid line.

model parameters was implemented by calculating the ratio between the behavioral parameter range to the initial range of each of the 9 parameters of model 3. Since four of the parameters (s_0, f, q_e, q_p) are fractions, their range of variability included all possible values and varied between 0 and 1 (Table 2). The initial ranges for the four transit time constants (k_{fe}, k_{se}, k_{fp}, and k_{sp}) and for the w parameter were set very wide to ensure capturing all range of variability. The selected ranges are only partially arbitrary; for the four time constants, the initial range was taken to be significantly longer than the interval over which the data were collected. If time constants are nonidentifiable in that interval, they cannot become identifiable in a broader interval since our data would not allow us to be sensitive to time constants longer than the time over which the data were collected. However, this does add a level of arbitrariness to our identification measure. We set up an arbitrary threshold for this ratio of 0.35 to discriminate between identifiable (MI < 0.35) and nonidentifiable parameters (MI > 0.35).

3.5. Patterns of Parameter Variability

[26] Pearson correlation was used to evaluate relationships between identifiable parameters values and catchment area, rainstorm size and intensity, and antecedent moisture conditions. These relationships were explored using best values of well-identified parameters in each catchment-storm pair. Since more than one storm was analyzed in each catchment (with the exception of SB), the best catchment-specific value and corresponding uncertainties were also derived by combining results from different storms. The probability distribution (p) of a catchment-specific parameter was obtained by convolving and rescaling the probability distribution of the parameter from each storm using equations (14) and (15):

$$p(x+y) = p(x) * p(y), \tag{14}$$

$$p(\alpha x) = \alpha p(x/\alpha), \tag{15}$$

where x and y are two independent stochastic variables ($p(x, y) = p(x)p(y)$), the symbol $*$ represent the convolution operator, and α is a constant [*Grinstead and Snell*, 1997]. An analogous procedure was applied to derive a probability distribution of storm-specific parameters across different catchments. Our average parameters for catchment or storms (i.e., convolved) were derived only after ensuring that the individual probability distributions were in agreement with each other (i.e., they overlap).

4. Results

4.1. Comparison of Model Performance

[27] An evaluation of model performance was performed using a subset of 13 catchment-storm pairs selected across all four storms and a range of catchment sizes (Figure 5). These initial runs indicated that the streamflow and tracer response of most of the catchment-storm pairs (10 out of 13) were well fit by all models, with the best fit of any of the models yielding a mean NS (Q, $\delta^{18}O$) > 0.85, our behavioral threshold. However, there were three catchment-rainstorm pairs (AW-8, AW-11, and SB-8) where model 1 with a constant fraction of effective precipitation routed as event water (f) and a single reservoir for event and preevent water routing were rejected as nonbehavioral

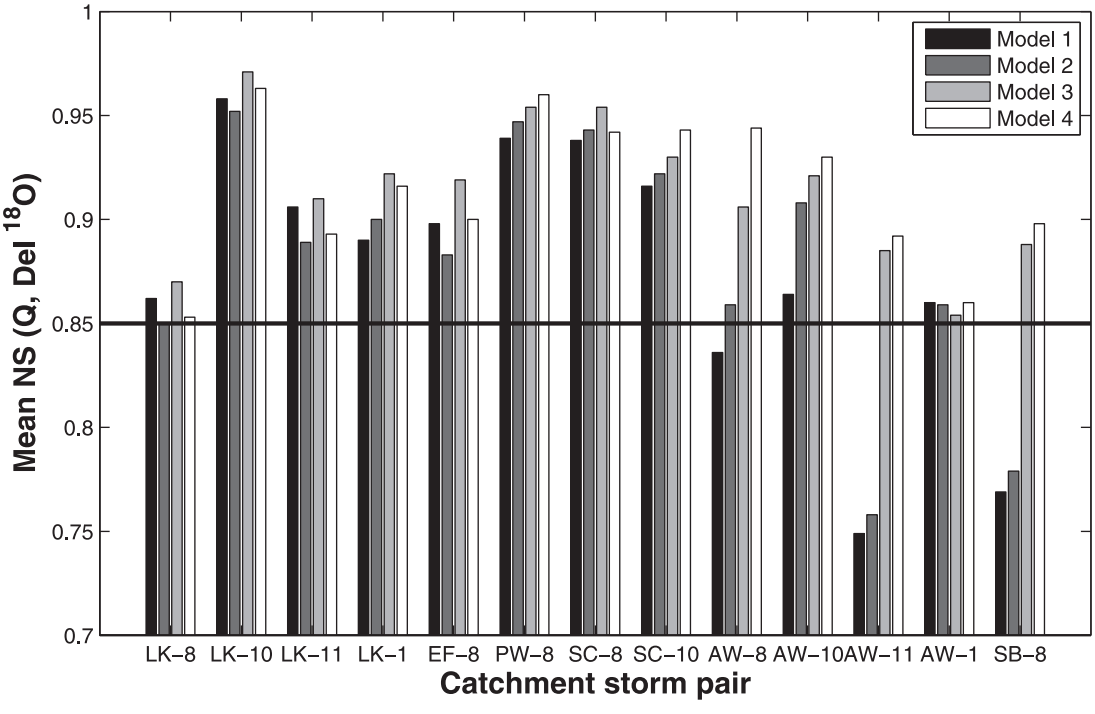

Figure 5. Best mean Nash-Sutcliffe (Q, $\delta^{18}O$) for four models and 13 catchment-storm pairs. Catchment-storm pairs identified by catchment acronym (e.g., LK) and storm number (e.g., 8) as shown in Table 1. The behavioral threshold (mean NS > 0.85) is displayed a thick line.

(i.e., NS < 0.85) (Figures 5). Model 2, also with a single reservoir for event and preevent water routing but with variable f, was inadequate (i.e., NS < 0.85) in two of the mentioned cases (AW-l1 and SB-8). Figures 6 and 7 present observations and all behavioral solutions for two of these three cases. In Figure 6, visual inspection of the time series of observed and predicted streamflow and $\delta^{18}O$ compositions for catchment-storm pair SB-8 indicates that models 1 and 2 provided a poor fit to both streamflow and $\delta^{18}O$ (Figures 6 and 7, left). These two models did not produce any behavioral sets of parameters (Figure 6 presents the best 100 simulations for these 2 models). Only the models with two reservoirs in parallel for each event and preevent water (Models 3 and 4) are able to capture the streamflow and $\delta^{18}O$ tracer response during the recession limb of the storm hydrograph (Figures 6 and 7, bottom right). The fits of the 4 models to the data in AW-8 (not shown here for brevity) displayed a very similar situation with model 1 failing to reproduce the response of both streamflow and $\delta^{18}O$. For catchment-storm pair AW-l1 (Figure 7) models 1 and 2 with a single reservoir each for event and preevent water routing cannot capture the double peak of streamflow (Figure 7, top left, where best 100 simulations are shown) while models 3 and 4 can (Figure 7, top right). In all these catchment-storm pairs, a fast and slow reservoir for both event and preevent water (4 reservoirs) provided a better performing model. It is interesting to note that these three catchment-storm pairs where Models 1 and 2 performed poorly correspond to the smaller (7–11 ha) catchments.

[28] We evaluated model parsimony for these 13 catchment-storm pairs using the AIC [*Akaike*, 1974] with the χ^2 statistic as a measure of likelihood (equation (12) and (13), Table 3). Model 3 was the best for 12 of the 13 catchment-storm pairs and model 1 was best for the remaining one. This analysis also indicated that model 4 with time-variable f (fraction of effective rainfall routed as event water) did not provide a superior fit to model 3 with constant f (Table 3) for any catchment-storm pairs. Models 1 and 2 had similar ranking positions for most catchment-storm pairs. Based on these preliminary results only model 3 was considered for the remaining 10 catchment-storm pairs. This model is therefore the only model included in the discussion of parameter identification and comparison across all rainstorms and catchments.

[29] Model results using model 3 for all catchment-storm pairs are presented in Tables 4 and 5. The best mean NS (Q, $\delta^{18}O$) for the 23 catchment-rainstorm pairs varied between 0.87 and 0.98 (Table 4). In most cases (17 out 23) NS for streamflow was higher than for $\delta^{18}O$ (Table 4). The range of behavioral parameter values (5th, 50th, 95th and best value) for each catchment storm-pair is presented in Table 5.

4.2. Model 3 Parameter Identification

[30] We evaluated the identification of behavioral and best model parameters using the GLUE methodology [*Freer et al.*, 1996] for all model 3 runs (Table 6). Dotty plots of model 3 parameters (illustrating individual NS for Q and $\delta^{18}O$ and mean NS for each model parameter) showed similar parameter identification for all catchment-storm pairs (Table 6), illustrated here by catchment-storm pair SB-8 (Figure 8). Similar to the findings of *Weiler et al.* [2003], best parameters values of s_0, and w (equation (2)) of the effective rainfall module $s(t)$ were not well defined for any catchment-storm pair due to weak sensitivity of the mean objective function to changes in parameter values. Similar behavior was observed for streamflow and $\delta^{18}O$ individually. This is shown in Figure 8 by the relatively uniform upper limits for mean NS (Q and $\delta^{18}O$) and individual lines for best Q and $\delta^{18}O$, respectively. The measure of identification (MI, i.e., ratio of behavioral parameter

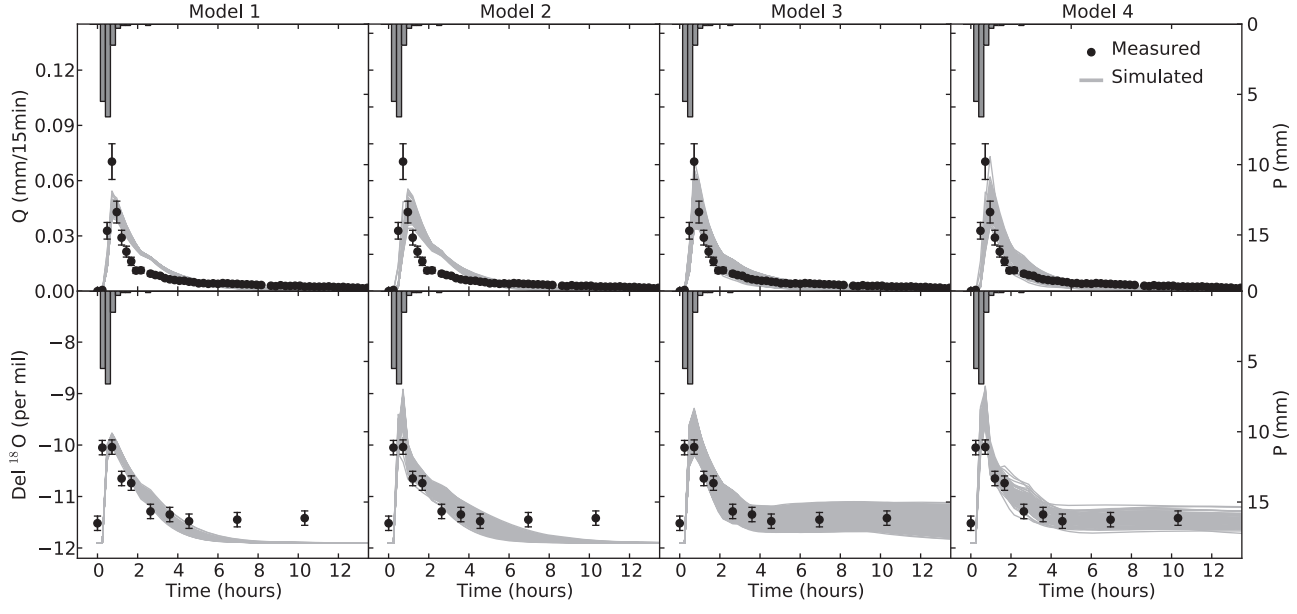

Figure 6. SB-8 catchment-storm pair comparison between observed values of streamflow (Q) and $\delta^{18}O$ compositions (symbols) and predictions (gray lines) for each model structure. For models 1 and 2 the best 100 runs are presented in the absence of behavioral solutions (see Figure 5). For models 3 and 4 all behavioral runs are shown.

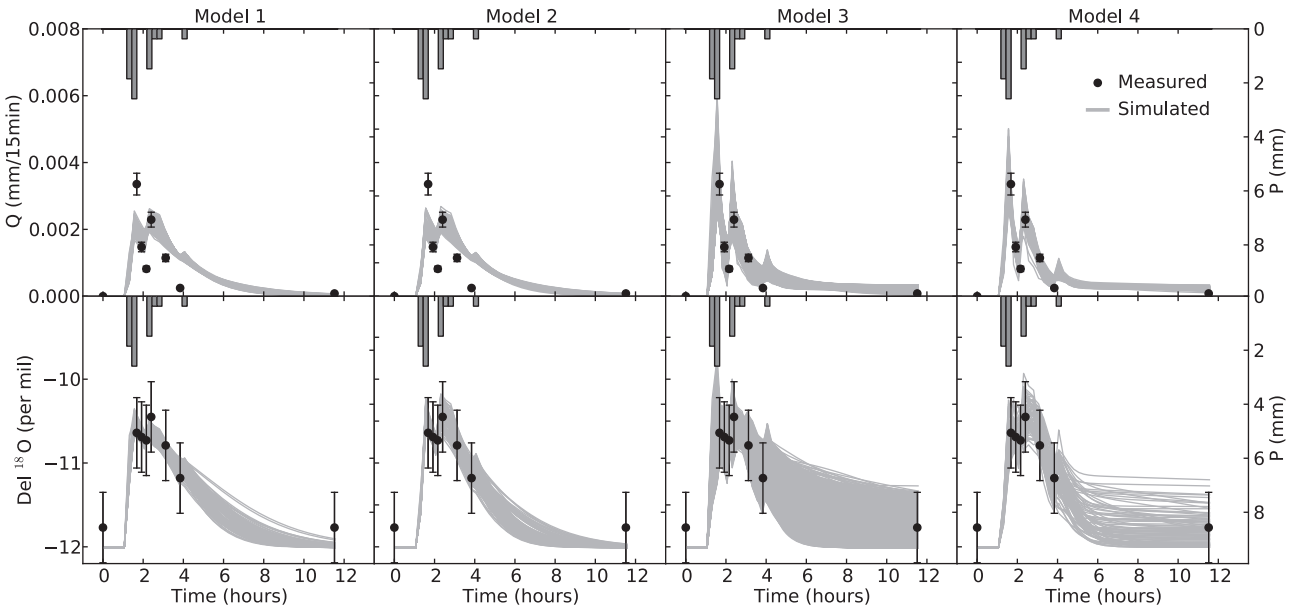

Figure 7. AW-11 catchment-storm pair comparison between observed values of streamflow (Q) and $\delta^{18}O$ compositions (symbols) and predictions (gray lines) for each model structure. For models 1 and 2 the best 100 runs are presented in the absence of behavioral solutions (see Figure 5). For models 3 and 4 all behavioral runs are shown.

range to initial parameter range) of s_0 was always above 51.5% with a mean of 87.1% (Table 6). For w the identification was also poor with only 3 out of 23 cases having MI below 35% (Table 6). Parameter f (Figure 8c) that defines the fraction of effective rainfall routed as event water was consistently well defined for all catchment-rainstorm pairs (with MI below 35% in all cases and an average of 16.2%). This parameter is especially well defined for $\delta^{18}O$ (Figure 8). Best f values varied between 0.19 and 0.77 (Table 6) indicating that for all catchment-storm pairs there are both event and preevent water components to stormflow. Some of the parameters that define the event and preevent transfer functions were well identified. The mean fast reservoir transit time of event (k_{fe}) and preevent water (k_{fp}) were both well defined, k_{fe} is well defined in all 23 cases whereas k_{fp} is well defined in 22 (see Table 6). These two parameters, k_{fe} and k_{fp} varied between 0.32–2.61 h, and 0.04–6.1 h, respectively, with no significant difference them ($p = 0.24$) (Tables 5 and 6 and Figure 8, for SB-8 example). Conversely, neither slow transit times of event (k_{se}) and preevent water (k_{sp}) are well defined (note the log scale on k_{se} and k_{sp} axes in Figure 8), which could be the result of short simulation times focused on a single hydrograph recession [*Weiler et al.*, 2003].

Table 3. Model Ranking of AIC Test for 13 Catchment-Storm Pairs Included in Preliminary Model Evaluation

Catchment-Storm Pair	Model 1	Model 2	Model 3	Model 4
LK-8	4	3	1	2
LK-10	4	3	1	2
LK-11	3	2	1	4
LK-1	4	3	1	2
EF-8	3	2	1	4
PW-8	3	4	1	2
SC-8	4	3	1	2
SC-10	4	3	1	2
AW-8	3	4	1	2
AW-10	1	3	2	4
AW-11	3	2	1	4
AW-1	4	3	1	2
SB-8	3	4	1	2

Table 4. Nash-Sutcliff Model Performance for All 23 Catchment-Storm Pairs for Model 3

Catchment-Storm Pair	Number of Behavioral Models	Best NS[a]		
		Q	$\delta^{18}O$	Average (Q, $\delta^{18}O$)
LK-8	6906	0.885	0.852	0.868
LK-10	8576	0.973	0.971	0.972
LK-11	4648	0.891	0.929	0.910
LK-1	11,273	0.952	0.914	0.933
EF-8	11,636	0.940	0.897	0.919
EF-10	9708	0.981	0.894	0.938
EF-11	1028	0.912	0.867	0.890
PW-8	25,546	0.973	0.939	0.956
PW-10	16,007	0.974	0.910	0.942
PW-11	1044	0.863	0.929	0.896
SC-8	5704	0.954	0.953	0.954
SC-10	1288	0.971	0.888	0.930
SC-11	1484	0.973	0.914	0.944
SC-1	7292	0.969	0.940	0.954
YV-8	2011	0.989	0.969	0.979
YV-1	1053	0.914	0.942	0.928
VC-8	4456	0.967	0.933	0.950
VC-10	14,403	0.938	0.955	0.947
AW-8	1010	0.885	0.987	0.936
AW-10	1118	0.936	0.902	0.919
AW-11	3771	0.912	0.945	0.928
AW-1	1111	0.889	0.854	0.872
SB-8	1062	0.884	0.916	0.900

[a]Total streamflow, Q; tracer composition, $\delta^{18}O$; average of Q and $\delta^{18}O$.

Table 5. Percentiles and Best Parameters Values for at Least 1000 Behavioral Parameter Sets for 23 Catchment-Storm Pairs[a]

	STORM 1				STORM 8				STORM 10				STORM 11			
Parameter	5%	50%	95%	Best	5%	50%	95%	Best	5%	50%	95%	Best	5%	50%	95%	Best
								SB								
s_0					0.04	0.40	0.92	0.05								
W					4.67	21.02	37.58	16.67								
F					0.28	0.33	0.39	0.33								
q_e					0.26	0.50	0.68	0.50								
k_{fe}					0.44	0.59	0.78	0.50								
k_{se}					5.51	22.45	94.4	14.69								
q_{ep}					0.18	0.65	0.95	0.20								
k_{fp}					0.80	1.54	2.10	0.60								
k_{sp}					2.08	9.84	102.0	3.60								
								AW								
s_0	0.01	0.19	0.84	0.00	0.01	0.14	0.95	0.75	0.06	0.54	0.95	0.61	0.10	0.58	0.96	0.69
w	0.50	0.59	0.66	0.48	0.39	0.58	20.49	2.12	0.67	1.29	3.26	1.55	3.92	20.65	37.99	33.63
f	0.76	0.83	0.91	0.77	0.14	0.20	0.38	0.29	0.49	0.55	0.62	0.52	0.19	0.23	0.31	0.28
q_e	0.13	0.57	0.92	0.97	0.14	0.42	0.91	0.28	0.29	0.70	0.95	0.82	0.17	0.43	0.89	0.36
k_{fe}	0.29	0.61	0.74	0.72	0.19	0.50	0.94	0.35	0.25	0.48	0.77	0.45	0.22	0.57	0.94	0.32
k_{se}	0.78	6.42	76.9	16.07	0.89	10.59	41.9	16.42	0.85	11.10	101.9	7.14	1.03	9.01	91.0	6.66
q_{ep}	0.05	0.49	0.95	0.68	0.03	0.12	0.41	0.07	0.14	0.50	0.94	0.37	0.08	0.22	0.37	0.13
k_{fp}	3.93	24.97	47.6	24.75	0.06	0.51	2.79	0.11	0.12	0.40	0.88	0.15	0.20	0.31	0.43	0.23
k_{sp}	12.80	55.8	114.4	29.5	5.77	11.38	41.2	5.89	0.64	8.00	90.1	3.43	4.51	16.63	88.1	41.3
								VC								
s_0					0.03	0.40	0.92	0.05	0.04	0.44	0.93	0.00				
w					3.66	21.06	38.33	14.63	4.01	21.56	38.16	33.13				
f					0.42	0.54	0.66	0.55	0.34	0.43	0.53	0.42				
q_e					0.17	0.69	0.97	0.93	0.18	0.70	0.97	0.93				
k_{fe}					0.63	1.04	1.52	1.04	0.37	0.80	1.32	0.94				
k_{se}					1.17	10.11	105.3	7.07	0.92	6.73	100.2	5.56				
q_{ep}					0.15	0.64	0.97	0.11	0.11	0.59	0.96	0.19				
k_{fp}					0.26	1.15	2.46	1.12	1.40	4.39	10.49	2.69				
k_{sp}					1.07	8.81	101.5	1.20	4.35	20.71	105.4	73.9				
								YV								
s_0	0.05	0.49	0.95	0.35	0.01	0.13	0.94	0.07								
w	1.61	17.49	37.52	11.60	0.39	0.61	30.24	0.46								
f	0.26	0.31	0.36	0.32	0.30	0.38	0.49	0.42								
q_e	0.21	0.78	0.97	0.50	0.16	0.52	0.92	0.37								
k_{fe}	0.45	0.70	0.93	0.59	0.08	0.55	1.38	0.77								
k_{se}	0.78	9.89	105.8	66.2	0.87	4.01	39.5	49.3								
q_{ep}	0.12	0.60	0.96	0.50	0.11	0.47	0.94	0.37								
k_{fp}	0.44	1.08	1.55	0.71	0.05	0.44	1.64	0.38								
k_{sp}	1.41	8.54	94.5	11.74	0.78	2.86	37.5	1.75								
								SC								
s_0	0.05	0.49	0.95	0.16	0.09	0.63	0.96	0.04	0.07	0.56	0.95	0.12	0.04	0.50	0.95	0.20
w	2.42	19.94	38.02	25.94	0.80	13.97	37.37	0.53	1.05	14.60	36.98	1.55	0.60	1.29	3.55	1.21
f	0.23	0.32	0.42	0.31	0.30	0.41	0.60	0.36	0.36	0.46	0.63	0.52	0.29	0.41	0.64	0.40
q_e	0.18	0.64	0.97	0.75	0.14	0.36	0.71	0.45	0.19	0.53	0.92	0.46	0.13	0.58	0.95	0.81
k_{fe}	0.55	0.93	1.41	1.14	0.08	0.33	0.66	0.52	0.27	0.72	1.16	0.55	0.09	0.29	0.46	0.34
k_{se}	1.02	14.84	104.8	61.0	1.03	5.26	35.8	1.78	1.20	6.25	41.7	23.45	0.34	14.61	101.5	35.5
q_{ep}	0.10	0.50	0.95	0.14	0.11	0.56	0.96	0.95	0.11	0.53	0.95	0.20	0.07	0.33	0.85	0.06
k_{fp}	1.47	4.49	9.71	0.76	1.31	4.37	12.40	6.11	1.12	4.29	10.57	1.76	0.03	0.23	0.43	0.04
k_{sp}	5.63	23.43	107.4	14.58	4.29	21.51	106.0	19.54	4.88	24.43	104.0	76.5	0.44	9.90	83.0	10.58
								PW								
s_0					0.06	0.53	0.96	0.17	0.03	0.44	0.94	0.30	0.14	0.60	0.95	0.48
w					2.04	19.59	37.89	19.85	1.64	17.39	37.56	3.14	8.32	24.71	38.24	24.27
f					0.22	0.30	0.38	0.34	0.47	0.55	0.64	0.60	0.17	0.19	0.22	0.19
q_e					0.16	0.62	0.96	0.48	0.13	0.69	0.97	0.53	0.10	0.72	0.97	0.70
k_{fe}					0.51	1.36	2.41	1.44	0.23	0.80	1.44	0.32	1.18	1.98	2.62	1.97
k_{se}					1.52	10.22	102.0	49.8	1.02	2.07	37.7	1.91	2.16	12.06	106.1	83.0
q_{ep}					0.12	0.58	0.96	0.36	0.11	0.55	0.95	0.62	0.14	0.49	0.93	0.33
k_{fp}					1.56	3.85	6.93	2.02	0.49	1.63	3.17	1.32	1.03	2.10	2.95	1.01
k_{sp}					4.32	19.95	106.3	35.4	1.82	8.72	42.5	9.01	3.22	16.55	104.7	10.26

Table 5. (continued)

	STORM 1				STORM 8				STORM 10				STORM 11			
Parameter	5%	50%	95%	Best	5%	50%	95%	Best	5%	50%	95%	Best	5%	50%	95%	Best
								EF								
s_0					0.07	0.55	0.96	0.69	0.09	0.52	0.94	0.21	0.03	0.34	0.91	0.05
w					2.73	20.27	37.82	30.70	4.64	21.45	38.25	18.47	5.61	20.07	37.36	33.47
f					0.25	0.30	0.35	0.30	0.46	0.53	0.60	0.47	0.18	0.20	0.22	0.21
q_e					0.19	0.68	0.97	0.74	0.16	0.69	0.97	0.68	0.22	0.61	0.94	0.50
k_{fe}					1.20	1.84	2.58	1.81	0.75	1.38	1.89	1.23	1.46	2.00	2.52	1.62
k_{se}					2.08	13.35	103.8	6.59	1.59	8.84	103.7	95.6	2.42	19.23	104.7	22.33
q_{ep}					0.12	0.58	0.96	0.38	0.11	0.56	0.96	0.16	0.14	0.63	0.96	0.51
k_{fp}					1.31	3.17	5.22	1.48	0.65	2.17	4.71	0.09	2.15	4.01	5.29	3.53
k_{sp}					3.65	17.52	104.0	9.56	2.42	16.44	104.7	26.4	4.51	21.80	108.0	124.7
								LK								
s_0	0.06	0.60	0.97	1.00	0.47	0.83	0.99	0.90	0.07	0.54	0.96	0.11	0.04	0.42	0.93	0.00
w	4.88	25.76	38.67	29.67	5.55	22.56	38.16	28.10	2.81	20.39	38.02	15.01	4.91	21.48	38.14	23.23
f	0.38	0.47	0.55	0.51	0.28	0.32	0.36	0.33	0.43	0.54	0.67	0.52	0.19	0.24	0.28	0.23
q_e	0.19	0.60	0.95	0.22	0.26	0.70	0.96	0.72	0.13	0.71	0.97	0.86	0.14	0.61	0.96	0.32
k_{fe}	1.16	2.14	3.35	1.48	2.05	2.49	2.95	2.61	0.91	1.71	2.66	1.45	1.80	3.30	4.99	2.54
k_{se}	2.75	20.07	106.0	119.9	2.85	26.8	110.7	35.0	1.88	8.75	101.8	24.53	3.68	17.90	106.8	87.5
q_{ep}	0.15	0.59	0.95	0.45	0.02	0.09	0.19	0.11	0.13	0.60	0.96	0.38	0.16	0.59	0.96	0.42
k_{fp}	1.03	2.43	3.93	1.36	0.15	0.52	0.90	0.64	0.60	2.48	6.06	0.70	1.33	2.86	3.98	2.19
k_{sp}	2.84	16.87	104.5	16.52	3.76	5.47	9.61	4.78	2.43	14.52	103.0	19.61	3.52	17.16	106.2	15.19

[a]Well identified parameters appear in bold. Empty cells indicate storms not included or available for analysis. Parameters Units as in Table 2.

than the mean fast transit time (k_{fe} and k_{fp}). The fraction of event (q_e) or preevent water (q_p) routed through the fast reservoir were not well defined in the majority of catchment-rainstorm pairs (Table 6).

[31] The best parameter value and its degree of identification depend on the objective function selected [*Son and Sivapalan*, 2007], in this case, the mean NS (Q, $\delta^{18}O$) giving equal importance to the fit of streamflow and $\delta^{18}O$. The NS calculated solely based on streamflow or $\delta^{18}O$ were examined for sensitivity of results to this selection (dark and light lines, respectively, in Figure 8 for SB-8 example). For SB-8 the best values of parameters f and k_{fe} are similar when identified by either streamflow or $\delta^{18}O$. For parameter k_{fp} best parameter values differ depending on which of the two objective functions is used. In this example the best value of k_{fp} based on Q is ~0.5 h; ~7.3 h when based on $\delta^{18}O$ alone, and ~1.5 h when both objective functions are considered. This indicates that a model based solely on streamflow or $\delta^{18}O$ would lack important information gained only when both objective functions are incorporated. Close analysis of the dotty plots and measure of identification (MI) of all 23 rainstorms revealed that in the 3 instances (Table 6) where w was well defined by the mean NS it was also well defined by streamflow and $\delta^{18}O$ alone, but in one of these cases the two objective functions were not in agreement. f was defined based on both $\delta^{18}O$ and streamflow and both measures were in agreement, however the MI for $\delta^{18}O$ was considerably lower (between 4 and 30) than for streamflow (between 7 and 43), indicating that $\delta^{18}O$ was able to constrain the parameter space in a higher degree than streamflow in most catchment-storm pairs (87%). Parameter k_{fe} was well defined by both objective functions in all catchment-storm pairs and both objective functions were in agreement. The MI of both objective functions was very similar and varied between 0.6 and 10. Finally k_{fp} was well defined by both objective functions in all cases except for AW-1 where neither was able to constrain the parameter and in SC-1 where neither streamflow nor $\delta^{18}O$ constrain the parameter space. In all cases both objective functions were in agreement and in 89% of the catchment-storm pairs streamflow gave a higher constrain of the parameter space than $\delta^{18}O$.

Table 6. Model 3 Parameter Ranges for All Catchment-Storm Pairs and Relative Parameter Identification[a]

Parameter	Initial Range	Range of Best Values	Identification Measure (MI)[b]	No. Storms Sith MI< 35%
s_0 (fraction)	0–1	0.00–1.00	87.1 (8.3)	0
w (15 min time steps)	0–40	0.46–33.6	73.0 (28.5)	3
F (fraction)	0–1	0.19–0.77	16.2 (7.9)	23
q_e (fraction)	0–1	0.22–0.97	75.3 (9.7)	0
K_{fe} (h)	0–50	0.32–2.61	2.2 (1.3)	23
k_{se} (h)	0–125	1.78–119.9	65.9 (10.1)	0
q_p (fraction)	0–1	0.06–0.95	75.5 (19.3)	2
K_{fp} (h)	0–50	0.04–6.11[b]	10.8 (17.8)	22
k_{sp} (h)	0–125	1.20–124.74	54.5 (14.9)	2

[a]The measure of identification (MI) corresponds to the average percent of initial parameter space covered between the 5th and 95th percentile of behavioral simulations (standard deviations in parenthesis).

[b]Excluding AW-1 because it is the only catchment-storm pair with this time constant not well identified.

4.3. Patterns of Parameter Variability Across Catchment-Storm Pairs

[32] Model parameters showed significant differences for the 23 catchment-storm pairs that represent variability in catchment response in both space and time. To further investigate this variability, the three consistently well-identified model parameters (f, k_{fe}, and k_{fp}) were evaluated as a function of catchment area, rainstorm size, and intensity and antecedent moisture conditions (i.e., antecedent precipitation index for 7, 14, and 25 days). This evaluation was

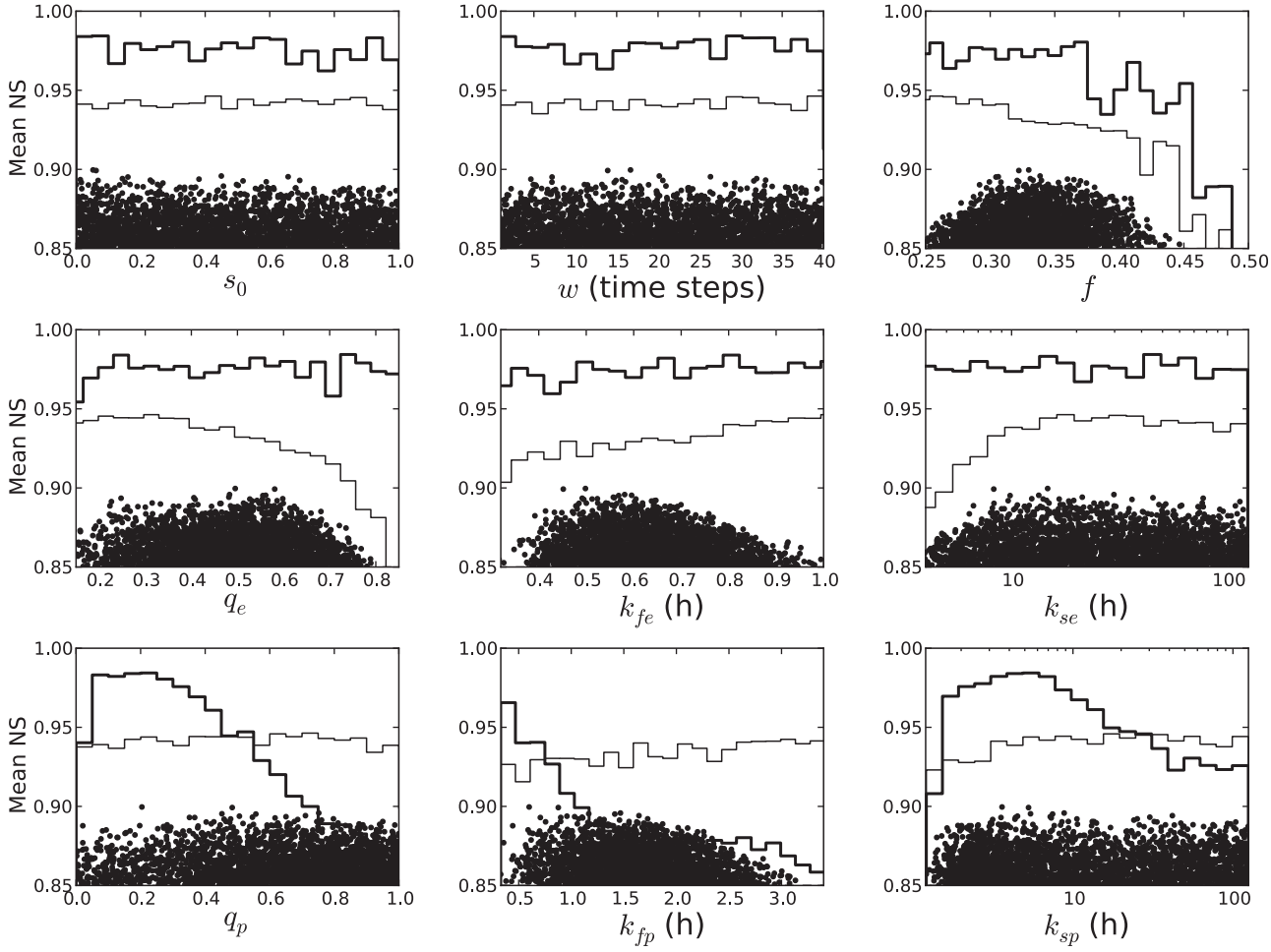

Figure 8. Dotty plots of model 3 parameters for catchment-storm pair SB-8. Note that the*y* axis starts at the behavioral threshold (mean NS = 0.85). There are 1062 behavioral runs for this catchment-storm pair. The thick line represents the maximum NS for streamflow (Q) alone and the lighter line, the maximum NS for $\delta^{18}O$ alone. Each dot represents the mean NS (Q and $\delta^{18}O$) for one behavioral run.

performed using Pearson correlation for both best and convolved values. The convolved distributions of well identified parameters with respect to catchment and storm are presented in Tables 7 and 8, respectively. The fraction of effective rainfall routed as event water (f) was observed to increase with rainstorm size (Figure 9a and 9b, Table 9). This indicates that a larger fraction of the effective rainfall is routed to the stream during large rainstorms compared to small rainstorms. These correlations between storm size and f are significant for both for best values ($r = 0.64$, $p = 0.001$, Table 9) and convolved values ($r = 0.95$, $p = 0.04$, Table 9), and similar to that found by *James and Roulet* [2009] between the total % event water contributions and rainstorm size ($r = 0.68$, $p < 0.001$) as generated using traditional IHS. The best f values were also positively correlated to average and maximum rainstorm intensity (mm/15 min) ($r = 0.42$ to 0.46, $p = 0.029$ to 0.047, Table 9), generating higher fractions of event water with greater intensity. The fraction of effective rainfall routed as event water is similar across catchment sizes (Figures 10a and 10b) indicating that for these 23 catchment-storm pairs f appears to be scale-independent. The total percent of event water contributions per catchment-storm pair simulated by model 3 were in agreement with those found from the IHS analysis [*James and Roulet*, 2009] and varied between 7.8 ± 3.8% and 45.7 ± 1.8% (0.002 ± 0.00004 and 0.49 ± 0.039 mm). As reported by *James and Roulet* [2009], there is a weak positive correlation between catchment area and total event water (in millimeters) for the largest rainstorms that indicate increasing magnitudes of event water delivered with increasing catchment size. This may be due to a variety of mechanisms (increased surface overland flow, return flow, direct precipitation on larger stream reaches in valley-bottom areas) with the shift from zero and first-order streams to a larger downstream network [*Gomi et al.*, 2002] even within the 150 ha Westcreek watershed of MSH. However, these correlations are not statistically significant and a larger catchment-storm sample would be required to confirm their validity.

[33] We found that there are positive correlations between storm size and average storm intensity and percent event water ($r = 0.60$ to 0.86, $p < 0.002$, Table 9) and total event water in millimeters ($r = 0.55$ to 0.68, $p = 0.004$ to 0.006, Table 9) indicating that larger and more intense storms produce higher percent and amounts of new water.

[34] There is some evidence for decreasing mean transit time of the fast reservoir of event water (k_{fe}) with rainstorm

Table 7. Percentiles and Best Values of Convolved Distributions of Parameters With Identification Measure (MI) < 35% With Respect to Catchment

Catchment	Parameter	5%	50%	95%	Best
SB[a]	f (fraction)	0.28	0.33	0.39	0.33
SB[a]	k_{fe} (h)	0.44	0.59	0.78	0.50
SB[a]	k_{fp} (h)	0.80	1.54	2.10	0.60
AW	f (fraction)	0.37	0.41	0.46	0.40
AW	k_{fe} (h)	0.39	0.53	0.68	0.53
AW[b]	k_{fp} (h)	0.21	0.54	1.20	0.29
VC	f (fraction)	0.41	0.49	0.57	0.48
VC	k_{fe} (h)	0.63	0.94	1.27	0.91
VC	k_{fp} (h)	1.26	2.90	5.98	2.33
YV	f (fraction)	0.30	0.35	0.41	0.34
YV	k_{fe} (h)	0.37	0.63	1.06	0.62
YV	k_{fp} (h)	0.36	0.78	1.41	0.68
SC	f (fraction)	0.35	0.41	0.49	0.40
SC	k_{fe} (h)	0.39	0.57	0.76	0.56
SC	k_{fp} (h)	1.94	3.58	6.16	3.17
PW	f (fraction)	0.31	0.35	0.39	0.34
PW	k_{fe} (h)	0.94	1.40	1.85	1.38
PW	k_{fp} (h)	1.60	2.55	3.70	2.44
EF	f (fraction)	0.31	0.34	0.37	0.34
EF	k_{fe} (h)	1.39	1.74	2.09	1.73
EF	k_{fp} (h)	2.11	3.14	4.27	3.08
LK	f (fraction)	0.34	0.37	0.41	0.37
LK	k_{fe} (h)	1.99	2.43	2.88	2.39
LK	k_{fp} (h)	1.17	1.76	2.55	1.66

[a]Same as SB-8 because there was only one storm in the SB catchment.
[b]The convolution does not include Storm 1 because its identification measure was above 80%.

size (Figures 9c and 9d) for some of the catchments (LK, PW, EF, YV, and VC). Such behavior is probably due to increased connectivity (i.e., activation of more flowpaths) under wetter conditions. This correlation is marginally statistically significant for the best values of LK ($r = 0.89$, $p = 0.1$) and PW ($r = 0.99$, $p = 0.06$) and should be confirmed with a larger sample. There were two catchments (AW and SC) where k_{fe} is almost constant among all storms except for storm 1. k_{fe} also decreases with average storm intensity for the same catchments (LK, EF, PW, YV and VC) but this relationship (not shown here for brevity) is only marginally significant at the PW catchment ($r = 0.99$, $p = 0.08$). We tested for effects of the sampling resolution of streamflow and $\delta^{18}O$ and found it had no bearing on transit time of event water. Results show a positive correlation between best and convolved values of k_{fe} and catchment area ($r = 0.78 - 0.94$ $p \ll 0.0005$, Figures 10c and 10d, Table 9). For larger catchment areas $CA > 30$ ha, k_{fe} is a strong function of catchment area ($k_{fe} = 1.23^{*}\ln(CA)$-3.8) (Figure 10d). This fit has a χ^2 of 0.1698 ($p = 0.0177$). At smaller catchment areas the correlation is lost, and a constant value of $k_{fe} \sim 40$ min gives a better description to the data. One possible explanation for this behavior is that there are two underlying processes controlling the mean transit time. One process scales with the catchment area while the second does not. If the value of k_{fe} is the sum of the transit times set by the two processes, small catchments are dominated by the constant transit time, while the transit time that depends on the CA dominates larger catchments. The equation that describes the relation between CA and k_{fe} (Figure 10d) can also be written as $k_{fe} = 0.021^{*}(CA)^{0.95}$. The exponent is close to one and indicates that the travel time of event water grows in direct proportion to catchment area for basins above 30 ha.

[35] Finally, no significant trends were observed between the variation of the fast transit time of preevent water (k_{fp}) and rainstorm size, intensity, or catchment area (Figures 9 and 10 and Table 9). There is a weak positive correlation between the convolved values of k_{fp} and storm size (Figure 9f, $r = 0.93$ $p = 0.07$) that indicates that as the storms size increases the time constant of preevent fast reservoir increases.

Table 8. Percentiles and Best Values of Convolved Distributions of Parameters With Identification Measure (MI) < 35% With Respect to Storm

Storm	Parameter	5%	50%	95%	Best
1	f	0.44	0.48	0.52	0.48
1	k_{fe} (h)	0.80	1.09	1.42	1.05
1	k_{fp} (h)	1.52	2.68	4.46	2.41
8	f	0.32	0.35	0.39	0.35
8	k_{fe} (h)	0.90	1.09	1.29	1.08
8	k_{fp} (h)	1.34	1.99	3.06	1.84
10	f	0.47	0.51	0.55	0.51
10	k_{fe} (h)	0.75	0.98	1.22	0.97
10	k_{fp} (h)	1.64	2.70	4.21	2.49
11	f	0.22	0.26	0.30	0.25
11	k_{fe} (h)	1.23	1.61	2.00	1.59
11	k_{fp} (h)	1.34	1.84	2.27	1.85

5. Discussion

5.1. Comparison of Model Performance

[36] In this paper a conceptual model structure that incorporates the unit hydrograph and IHS methodologies was used to model storm-based streamflow and stable isotope tracer response from a series of forested catchments. Four versions of the model with increasing complexity were considered, ranging from the simplest (5 free parameters) with constant fraction of effective rainfall routed as event water (f) and a single-reservoir routing for event and preevent water, to the most complex (10 free parameters), with variable f and two parallel reservoirs routing for event and preevent water. Results indicated that a model structure with intermediate complexity and 9 free parameters was adequate in all 23 catchment-storm pairs modeled. The resulting model (model 3) was simple in terms of a constant fraction of effective rainfall routed as event water but retained the two linear parallel reservoirs for event and preevent water. The 4-reservoir structure (i.e., two parallel linear reservoirs, for each event and preevent water) was also found to be the most efficient in other conceptual model applications that incorporate tracer data [*Weiler et al.*, 2003; *Iorgulescu et al.*, 2005; *McGuire and McDonnell*, 2006; *Iorgulescu et al.*, 2007; *Johnson et al.*, 2007; *Hrachowitz et al.*, 2009]. Interestingly, in this study, the simplest model with just one reservoir gave an adequate result for most catchment-storm pairs. However, 3 catchment-storm pairs out of 13 located in the smallest catchments required an additional reservoir with a distinct mean transit time in order to meet the behavioral threshold of mean NS equal to 0.85. Addition of this model complexity was a direct result of including the $\delta^{18}O$ data set; the recession of $\delta^{18}O$ compositions illustrated the need for a fast and slow reservoir of event and preevent water for these catchment-storm pairs. The constant event water routing fraction

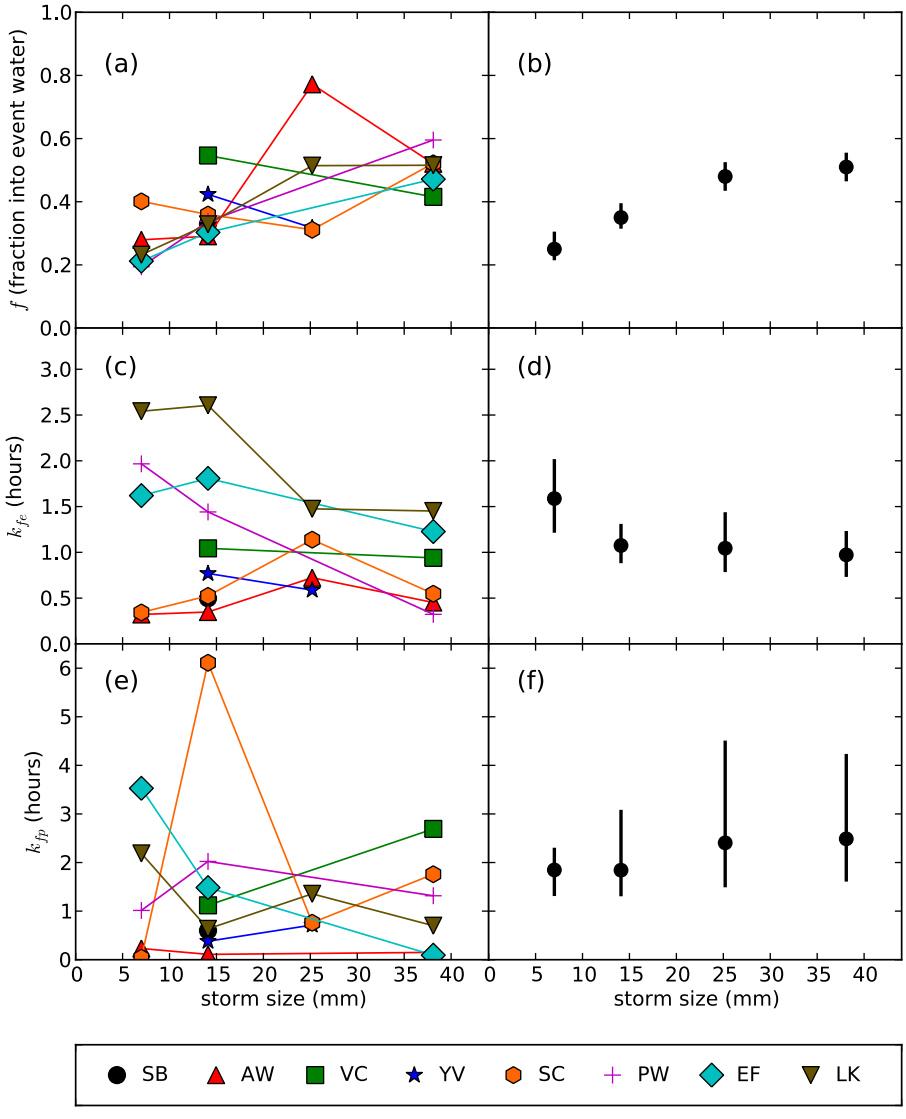

Figure 9. Relationships between storm size and the three identifiable parameters ((a and b) fraction of effective rainfall routed as event water, f; (c and d) mean transit time of the fast reservoir of event water, k_{fe}; and (e and f) mean transit time of the fast reservoir of preevent water, k_{fp}). Figures 9a, 9c, and 9e present best values per storm pair ($n = 23$). Figures 9b, 9d, and 9f present convolved distribution of parameters per storm. The filled circle is the best value and the deviation bars include all possible values between the 5th and 95th percentiles.

Table 9. Pearson Correlation Matrix of Catchment and Storm Characteristics Versus Best Parameters and Convolved Values of Well Identified Parameters and Event Water[a]

Catchment/Storm Characteristics	Parameters						Event Water	
	f (n = 23)	f Convolved	k_{fe} (n = 23)	k_{fe} Convolved	k_{fp} (n = 22)	k_{fp} Convolved	%	mm
Catchment area (ha)	−0.14 (0.517)	−0.267 (0.52)	**0.777 (<<0.00013)**	**0.94 (0.00053)**	0.081 (0.72)	0.34 (0.41)	−0.20 (0.35)	0.21 (0.34)
Storm size (mm)	**0.64 (0.0010)**	**0.95 (0.049)**	−0.27 (0.21)	−0.79 (0.20)	−0.12 (0.59)	0.93 (0.071)	**0.86 (<0.00010)**	**0.55 (0.0064)**
AI (mm/15 min)[b]	**0.42 (0.047)**	0.54 (0.46)	−0.21 (0.333)	−0.60 (0.40)	−0.030 (0.89)	0.42 (0.57)	**0.60 (0.0023)**	**0.68 (0.0035)**
Max.int (mm/15 min) [b]	**0.46 (0.029)**	0.71 (0.28)	−0.16 (0.474)	−0.69 (0.30)	−0.089 (0.69)	0.61 (0.38)	0.40 (0.06)	0.11 (0.62)
API_7 (mm)	−0.038 (0.86)	−0.034 (0.96)	−0.0086 (0.97)	−0.43 (0.56)	0.11 (0.62)	−0.37 (0.63)	−0.18 (0.40)	0.30 (0.16)
API_{14} (mm)	−0.066 (0.68)	−0.084 (0.92)	0.0019 (0.99)	−0.39 (0.61)	0.12 (0.60)	−0.41 (0.58)	−0.21 (0.33)	0.29 (0.18)
API_{25} (mm)	− 0.044 (0.86)	−0.0076 (0.99)	0.012 (0.96)	−0.47 (0.67)	−0.16 (0.51)	0.12 (0.40)	−0.27 (0.27)	0.12 (0.61)

[a]P-values are given in parenthesis. Significant relationships ($P < 0.05$) are in bold.
[b]AI = average storm intensity (mm/15 min); Max. int = maximum storm intensity (mm/15 min).

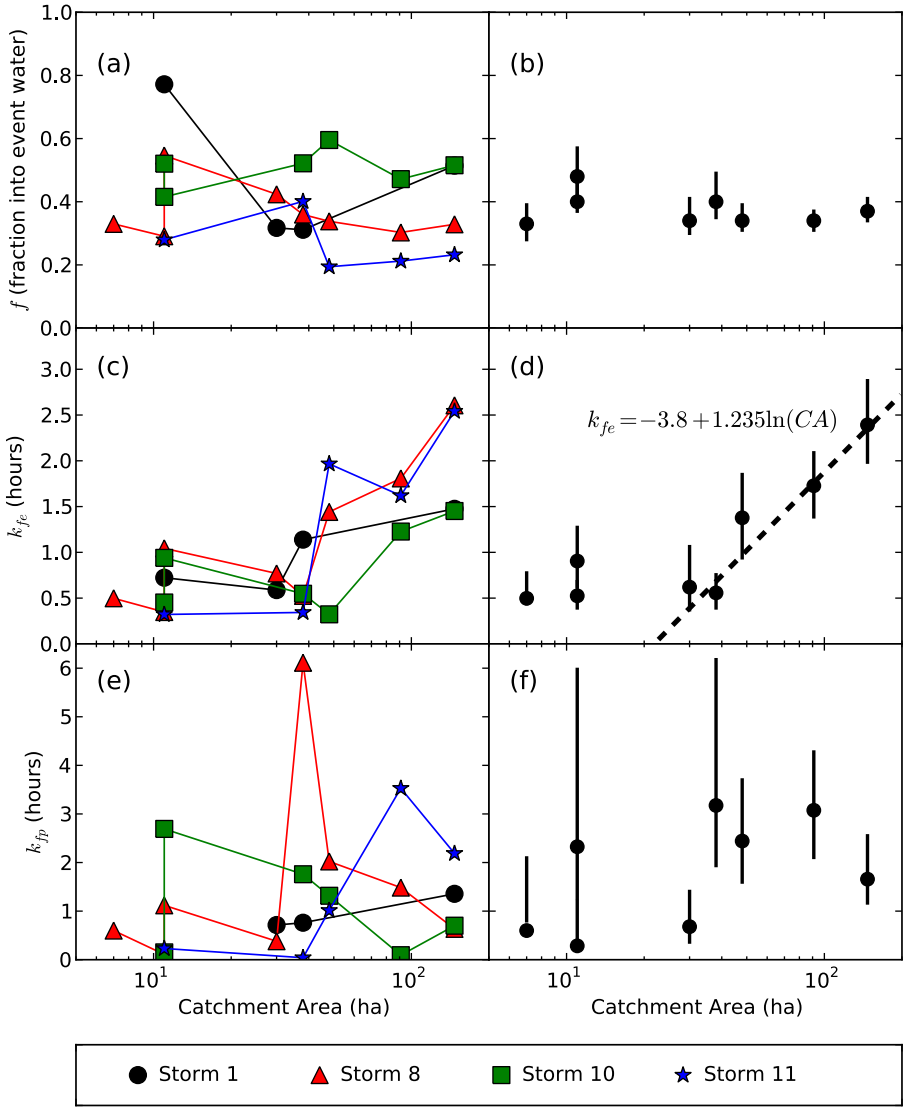

Figure 10. Relationships between catchment area and the three identifiable parameters ((a and b) fraction of effective rainfall routed as event water, f; (c and d) mean transit time of the fast reservoir of event water, k_{fe}; and (e and f) mean transit time of the fast reservoir of preevent water, k_{fp}). Figures 10a, 10c, and 10e present best values per catchment pair ($n = 23$). Figures 10b, 10d, and 10f present convolved distribution of parameters per catchment. The filled circle is the best value than the deviation bars include all possible values between the 5th and 95th percentiles.

that we found adequate contrasts with the results of *Weiler et al.* [2003], where the necessity of a varying fraction of effective rainfall routed as event water was emphasized. This difference in results may reflect a genuine difference in the active processes of runoff generation in the two locations or may be due to the different characteristics of the datasets used. While temporal variation in rainfall tracer compositions were available to *Weiler et al.* [2003], only a single spatially averaged throughfall tracer composition (volume-weighted average of 15 throughfall collectors) per rainstorm was available here.

5.2. Parameter Identification and Patterns of Parameter Variability

[37] The parameters of the final model structure show different degrees of identification. Parameters related to the nonlinear module that transforms throughfall into effective rainfall were poorly identified, whereas most of the parameters related to the routing section of the model were well constrained. Among the well-constrained parameters, the fraction of effective rainfall routed as event water (f) was correlated to rainstorm size and intensity, and the mean transit time of the fast reservoir of event water (k_{fe})was correlated to rainstorm size and catchment area. The mean transit time of the fast reservoir preevent water (k_{fp}), in contrast, did not display any correlation with rainstorm size nor catchment size. The positive correlation between f and rainstorm size is consistent with that found by *James and Roulet* [2009], who analyzed the same data set with traditional IHS techniques. Our results are also consistent with those of *Brown et al.* [1999] who observed strong dependence between the mean maximum contribution of event

water and mean maximum throughfall intensity and magnitude for 5 rainstorms in small (<2 km^2) forested catchments in New York during dry conditions ($r = 0.69$ to 0.96, $p = 0.009$ to 0.19) and *Renshaw et al.* [2003] who found a strong correlation between storm size and percent old water contribution ($r = 0.93$, $p < 0.0001$) for a fourth-order catchment (12 km^2 ha) in Etna, NH.

[38] Existing studies present inconclusive results on the trend of the fraction of effective rainfall routed as event water with catchment size [*Genereux and Hooper*, 1998]. Here, we did not find any significant trend with catchment area, in agreement with previous studies by *McGlynn et al.* [2004] in the Maimai catchment (catchments areas between 0.09 and 280 ha), and *Onda et al.* [2006] in small (1.2–6.3 ha) steep Japanese catchments. However, others reported relations between catchment size and event water contribution. *Brown et al.* [1999] found a negative correlation between maximum new water contribution and catchment area during 4 storm events in 7 forested New York catchments ($r = 0.21$ to 0.76, $p = 0.04$ to 0.45). *Shanley et al.* [2002], on the other hand, found weak positive correlations between percent new water input and catchment area for 4 storm events in 3 forested Vermont catchments ($r = 0.55$ to 0.82. $p = 0.38$ to 0.62) for varying catchment area (41–11,125 ha). More recently *Laudon et al.* [2007] found positive significant relations between percent new water input and catchment area for 13 Sweden boreal catchments (4–6700 ha) during the peak and falling limb of the snowmelt hydrograph ($r = 0.54$, $p = 0.04$ for both). The existence of a relation between percent event water contribution and catchment size as well as its direction (negative or positive) appears to vary with each catchment and set of conditions; site-specific studies themselves generate contrasting results [*Shanley et al.*, 2002; *Laudon et al.*, 2007].

[39] The mean transit time for the fast event water reservoir, k_{fe}, was found to be negatively correlated to rainstorm size in most catchments, indicating that the event water from larger rainstorms is routed faster than from smaller rainstorms. This correlation is likely due to increased connectivity in the catchment as rainstorm size increases [*Jencso et al.*, 2009]. Some of this connectivity at MSH is occurring in the shallow subsurface, as evidenced by strong correlations between $\delta^{18}O$ and dissolved organic carbon concentrations in stream water, indicating event water traveling through a shallow subsurface flowpath, particularly for the larger rainstorms during dry conditions [*James and Roulet*, 2009]. Previous studies at the hillslope scale have established that subsurface flow depends on available soil macropores, matrix and antecedent moisture conditions. Findings suggest that the soil porevolume depends on antecedent hydrologic conditions due to expansion of individual macropores with surrounding soil and the lateral extension of macropore networks during wet conditions [*Tsuboyama et al.*, 1994; *Sidle et al.*, 2000], however in our data AMC, only based on precipitation metrics, were unrelated to mean transit times (Table 9). This lack of correlation has to be taken with caution considering that only one of our four storms took place during the wet conditions [*James and Roulet*, 2009]. More recent studies have established that the subsurface flow is related to pore pressure, groundwater level, subsurface saturated area and permeability, especially during wet conditions [*Uchida et al.*, 2004]. In addition, others have found that total pipe flow volume was highly controlled by the total rainfall amount and the prestorm wetness [*Uchida et al.*, 2005]. This is in agreement with the decreasing trend we found between k_{fe} and storm size for most catchments.

[40] Transfer functions are known be nonstationary [*Hrachowitz et al.*, 2010; *Rinaldo et al.*, 2011] and we found evidence of such a behavior in the rainfall-runoff response of the 23 catchment-storm pairs that we analyzed. We found that the relative portion of event and preevent water (*f* parameter) was not constant, either among catchments or storms. Since the mean transfer times of event and preevent water are different, a variation of their relative fraction results in an overall variation of the transfer function for the total water. Analogous results were found in previous studies. *Iorgulescu et al.* [2005, 2007] found nonlinear and nonstationary behavior of the contributions of soil water and groundwater to storm response during a 5 week period for a 0.24 km^2 forested catchment. They found that relative contribution of the soil water and groundwater components varies with wetness conditions (i.e., from the wet to the dry seasons). For our data set, however, we did not find any evidence of the nonstationary behavior of the transfer function of event water (the transit time, k_{fe}, is constant across storms, see in Figures 9 and 10). Our results confirm the nonstationary behavior of the combined contributions of event and preevent water. The transfer function of event water (k_{fe}) is found to be stationary and its mean transit time linearly dependent on catchment area (for catchments above 30 ha).

[41] The correlation between k_{fe}, and catchment size is perhaps the most interesting of all (Figure 10d and Figure 11). It indicates that at MSH k_{fe} increases with catchment area for catchments between 30 and 150 ha. The magnitudes of k_{fe} at MSH are similar to other small headwater catchment studies. *Weiler et al.* [2003] found a mean transit time of the event water of 1.5 h for the Maimai basin (17 ha), *Roa-Garcia and Weiler* [2010] found mean transit times of the event water reservoir between 0.6 and 4.7 h for Andean catchments of areas between 62 and 159 ha, while *Lyon et al.* [2008] found a mean transit time of 4.5 h for a 880 ha catchment in Arizona. These results are comparable to those of MSH, and appear to emphasize a general trend of increasing k_{fe} with catchment area (Figure 11). This study provides an interesting perspective on the scaling of the runoff generation processes in small headwater systems. We found that the small catchments at MSH are those for which the highest degree of model complexity was required, consistent with observations of higher variability in streamflow, stream water chemistry, relative contribution of groundwater, and pH for smaller systems [*Wood et al.*, 1988; *Woods et al.*, 1995; *Wolock et al.*, 1997; *Bishop et al.*, 2008; *Asano et al.*, 2009; *Uchida and Asano*, 2010]. All these studies have found either asymptotic or convergent patterns in the relations between catchment area and runoff and infiltration [*Wood et al.*, 1988; *Woods et al.*, 1995]; solute concentrations [*Wolock et al.*, 1997; *Bishop et al.*, 2008; *Asano et al.*, 2009], and the relative contribution of bedrock [*Uchida and Asano*, 2010]. Here, we also found a difference in behavior between "small" and "large". While for larger catchments we found a linear relation between *CA* and k_{fe} (Figure 11) and a model with a simpler structure (i.e., Model 1) could describe the rainstorm-based runoff generation in these larger catchments, this relation was

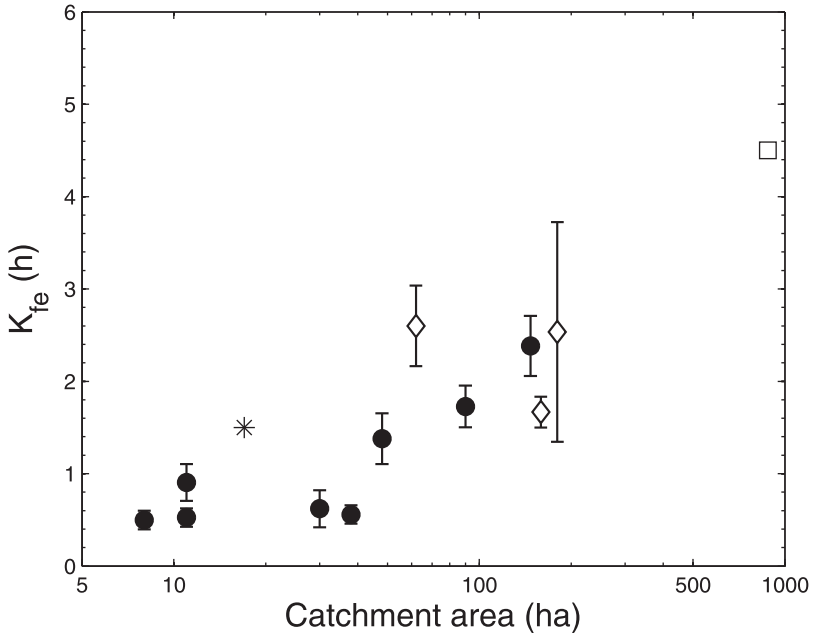

Figure 11. Comparison between the meant transit time of the fast reservoir of event water (k_{fe}) found in this study (black circles) to the Maimai catchment [*Weiler et al.*, 2003] (star symbol), Upper Sabino catchment [*Lyon et al.*, 2008] (square symbol), and Andean catchments [*Roa-Garcia and Weiler*, 2010] (diamond symbols).

absent in smaller catchments at MSH (i.e., 7–10 ha). These results suggest that understanding and predicting the hydrologic behavior for a small catchment is a much more challenging task than for a larger catchment, where the properties of the small building blocks are averaged out into a simpler mean configuration [*Bishop et al.*, 2008] with lesser degree of variability and complexity. Future steps should consider assembling studies of smaller catchments so that a collective populating of Figure 11 may help shed light on the behavior smaller systems.

6. Conclusion

[42] In this study catchment streamflow and $\delta^{18}O$ stable isotope tracer response were modeled using a conceptual model integrating the unit hydrograph and IHS methodologies. The model was applied across eight nested catchments for four individual rainstorms, generating a usable data set of 23 catchment-storm pairs. The data set spans variation both in space (i.e., catchment area between 11 and 147 ha) and time or environmental conditions (i.e., variable storm of size, storm intensity, and antecedent moisture conditions). Four model structures of varying complexity were evaluated using the GLUE methodology. The most successful model structure at replicating event-based streamflow and $\delta^{18}O$ included a constant fraction of effective rainfall routed as event water and two linear reservoirs in parallel for event and preevent water routing.

[43] We found that the fraction of effective rainfall routed as event water was correlated to rainstorm size but insensitive to catchment size indicating that this fraction is constant in all catchments and controlled by other environmental conditions such as storm intensity and size. The mean transit time of event water, k_{fe}, decreased with rainstorm size indicating that increased connectivity during strong rainstorm events decreased the mean travel time of event water. This relation was consistent with the activation of fast event water moving through the O-horizon under large rainstorms. At MSH, k_{fe}, is constant in the smallest catchments but increased with catchment size for catchments above 30 ha, indicating that travel time is larger for larger catchments. Comparison with three other empirical studies provides additional evidence of a general increasing trend in k_{fe} with catchment area. The relationships we found between some model parameters and rainstorm characteristics and catchments size constitute a step forward for the development of a predictive model of catchment response. Next steps include the application of this methodology to different scenarios (i.e., other catchments with different physiography) and conditions (i.e., different climates) to investigate the strength of the relationships found here.

Notation

P	Rainfall
P_{eff}	Effective rainfall
$s(t)$	Antecedent rainfall index
s_0	Initial value of $s(t)$
ω	Memory timescale parameter to compute $s(t)$
c	Normalization constant to maintain the water balance ($\Sigma P_{eff} = \Sigma Q$).
f	Fraction of effective rainfall routed as event water
$f(t)$	Time varying fraction of effective rainfall routed as event water
c_f	Free parameter to compute the $f(t)$
w_f	Memory timescale parameter to compute $f(t)$
$h_e(\tau)$, $h_p(\tau)$	Transfer function. This can be either event water ($h_e(\tau)$) or preevent water ($h_p(\tau)$)

k_e, k_p Mean transit time of a single linear reservoir. This can be either event water (k_e) or preevent water (k_p)

q_e, q_p Fraction of water routed into the fast reservoir of either the event (q_e) or preevent (q_p) water

k_{fe}, k_{fp} Mean transit times of the fast reservoir. This can be either event (k_{fe}) or preevent (k_{fp})

k_{se}, k_{sp} Mean transit times of the slow reservoir. This can be either event (k_{se}) or preevent (k_{sp})

$g(\tau)$ Total runoff transfer function

Q_e Event water contribution to streamflow

Q_p Preevent water contribution to streamflow

C Tracer concentration

C_p Tracer composition in the preevent water

C_e Tracer composition of event water

Q_b Base flow

Q Total stream flow

[44] **Acknowledgments.** This work was funded in part by the Department of Forestry and Environmental Resources, NC State University (NCSU). The authors would like to thank the NCSU College of Natural Resources information technology services group for computational support. Thanks also to Stacy Nelson for additional funding support. Additional thanks go to the Mont Saint-Hilaire, QC nature reserve and McGill University faculty and students for support of the original field campaigns and supporting LiDAR data set.

References

Akaike, H. (1974), A new look at the statistical model identification, *IEEE Trans. Autom. Control*, *19*(6), 716–723.

Asano, Y., T. Uchida, Y. Mimasu, and N. Ohte (2009), Spatial patterns of stream solute concentrations in a steep mountainous catchment with a homogeneous landscape, *Water Resour. Res.*, *45*, W10432, doi:10.1029/2008WR007466.

Atkinson, S. E., R. A. Woods, and M. Sivapalan (2002), Climate and landscape controls on water balance model complexity over changing timescales, *Water Resour. Res.*, *38*(12), 1314, doi:10.1029/2002WR001487.

Bai, Y., T. Wagener, and P. Reed (2009), A top-down framework for watershed model evaluation and selection under uncertainty, *Environ. Modell. Softw.*, *24*(8), 901–916.

Beven, K. J. (2001), *Rainfall-Runoff Modelling the Primer*, 360 pp., John Wiley and Sons, Chichester, U.K.

Beven, K. J. (2009), *Environmental Modelling: An Uncertain Future?*, 310 pp., Routledge, New York.

Bevington, P. R., and D. K. Robinson (2003), *Data Reduction and Error Analysis for the Physical Sciences*, McGraw-Hill, New York.

Birkel, C., D. Tetzlaff, S. M. Dunn, and C. Soulsby (2010), Towards a simple dynamic process conceptualization in rainfall-runoff models using multi-criteria calibration and tracers in temperate, upland catchments, *Hydrol. Processes*, *24*(3), 260–275.

Bishop, K., I. Buffam, M. Erlandsson, J. Folster, H. Laudon, J. Seibert, and J. Temnerud (2008), Aqua Incognita: The unknown headwaters, *Hydrol. Processes*, *22*(8), 1239–1242.

Bottomley, D. J., D. Craig, and L. M. Johnston (1984), Neutralization of acid runoff by groundwater discharge to streams in Canadian precambrian shield watersheds, *J. Hydrol.*, *75*(1–4), 1–26.

Brown, V. A., J. J. McDonnell, D. A. Burns, and C. Kendall (1999), The role of event water, a rapid shallow flow component, and catchment size in summer rainstorm flow, *J. Hydrol.*, *217*(3–4), 171–190.

Dingman, S. L. (1994), *Physical Hydrology*, Prentice-Hall, Upper Saddle River, N.J.

Eder, G., M. Sivapalan, and H. P. Nachtnebel (2003), Modelling water balances in an Alpine catchment through exploitation of emergent properties over changing time scales, *Hydrol. Processes*, *17*(11), 2125–2149.

Farmer, D., M. Sivapalan, and C. Jothityangkoon (2003), Climate, soil, and vegetation controls upon the variability of water balance in temperate and semiarid landscapes: Downward approach to water balance analysis, *Water Resour. Res.*, *39*(2), 1035, doi:10.1029/2001WR000328.

Fenicia, F., J. J. McDonnell, and H. H. G. Savenije (2008), Learning from model improvement: On the contribution of complementary data to process understanding, *Water Resour. Res.*, *44*(6), W06419, doi:10.1029/2007WR006386.

Franks, S. W., P. Gineste, K. J. Beven, and P. Merot (1998), On constraining the predictions of a distributed model: The incorporation of fuzzy estimates of saturated areas into the calibration process, *Water Resour. Res.*, *34*(4), 787–797.

Freer, J. E., K. J. Beven, and B. Ambroise (1996), Bayesian estimation of uncertainty in runoff prediction and the value of data: An application of the GLUE approach, *Water Resour. Res.*, *32*(7), 2161–2173.

Freer, J. E., H. McMillan, J. J. McDonnell, and K. J. Beven (2004), Constraining dynamic TOPMODEL responses for imprecise water table information using fuzzy rule based performance measures, *J. Hydrol.*, *291*(3–4), 254–277.

Genereux, D. P., and R. P. Hooper (1998), Oxygen and hydrogen isotopes in rainfall–runoff studies, in *Isotope Tracers in Catchment Hydrology*, edited by C. Kendall and J. J. McDonnell, pp. 319–346, Elsevier, Amsterdam.

Gomi, T., R. C. Sidle, and J. S. Richardson (2002), Understanding processes and downstream linkages of headwater systems, *Bioscience*, *52*(10), 905–916.

Grinstead, C. M., and J. L. Snell (1997), *Introduction to Probability*, 2nd ed., Am. Math. Soc., Providence, R.I.

Guntner, A., S. Uhlenbrook, J. Seibert, and C. Leibundgut (1999), Multicriterial validation of TOPMODEL in a mountainous catchment, *Hydrol. Processes*, *13*(11), 1603–1620.

Hrachowitz, M., C. Soulsby, D. Tetzlaff, J. J. C. Dawson, and I. A. Malcolm (2009), Regionalization of transit time estimates in montane catchments by integrating landscape controls, *Water Resour. Res.*, *45*, W05421, doi:10.1029/2008WR007496.

Hrachowitz, M., C. Soulsby, D. Tetzlaff, I. A. Malcolm, and G. Schoups (2010), Gamma distribution models for transit time estimation in catchments: Physical interpretation of parameters and implications for time-variant transit time assessment, *Water Resour. Res.*, *46*, W10536, doi:10.1029/2010WR009148.

Iorgulescu, I., K. J. Beven, and A. Musy (2005), Data-based modelling of runoff and chemical tracer concentrations in the Haute-Mentue research catchment (Switzerland), *Hydrol. Processes*, *19*(13), 2557–2573.

Iorgulescu, I., K. J. Beven, and A. Musy (2007), Flow, mixing, and displacement in using a data-based hydrochemical model to predict conservative tracer data, *Water Resour. Res.*, *43*, W03401, doi:10.1029/2005WR004019.

Jakeman, A. J., and G. M. Hornberger (1993), How much complexity is warranted in a rainfall-runoff model, *Water Resour. Res.*, *29*(8), 2637–2649.

Jakeman, A. J., I. G. Littlewood, and P. G. Whitehead (1990), Computation of the instantaneous unit-hydrograph and identifiable component flows with application to 2 small upland catchments, *J. Hydrol.*, *117*(1–4), 275–300.

James, A. L., and N. T. Roulet (2006), Investigating the applicability of end-member mixing analysis (EMMA) across scale: A study of eight small, nested catchments in a temperate forested watershed, *Water Resour. Res.*, *42*, W08434, doi:10.1029/2005WR004419.

James, A. L., and N. T. Roulet (2007), Investigating hydrologic connectivity and its association with threshold change in runoff response in a temperate forested watershed, *Hydrol. Processes*, *21*(25), 3391–3408.

James, A. L., and N. T. Roulet (2009), Antecedent moisture conditions and catchment morphology as controls on spatial patterns of runoff generation in small forest catchments, *J. Hydrol.*, *377*(3–4), 351–366.

Jeelani, G., N. A. Bhat, and K. Shivanna (2010), Use of delta(18)O tracer to identify stream and spring origins of a mountainous catchment: A case study from Liddar watershed, Western Himalaya, India, *J. Hydrol.*, *393*(3–4), 257–264.

Jencso, K. G., B. L. McGlynn, M. N. Gooseff, S. M. Wondzell, K. E. Bencala, and L. A. Marshall (2009), Hydrologic connectivity between landscapes and streams: Transferring reach- and plot-scale understanding to the catchment scale, *Water Resour. Res.*, *45*, W04428, doi:10.1029/2008WR007225.

Johnson, M. S., M. Weiler, E. G. Couto, S. J. Riha, and J. Lehmann (2007), Storm pulses of dissolved CO_2 in a forested headwater Amazonian stream explored using hydrograph separation, *Water Resour. Res.*, *43*, W11201, doi:10.1029/2007WR006359.

Kabeya, N., A. Shimizu, S. Chann, Y. Tsuboyama, T. Nobuhiro, N. Keth, and K. Tamai (2007), Stable isotope studies of rainfall and stream water in forest watersheds in Kampong Thom, Cambodia, in *Forest*

Environments in the Mekong River Basin, edited by H. Sawada et al., pp. 125–134, Springer, New York.

Kirchner, J. W. (2006), Getting the right answers for the right reasons: Linking measurements, analyses, and models to advance the science of hydrology, *Water Resour. Res.*, *42*, W03S04, doi:10.1029/2005WR004362.

Lamb, R., K. Beven, and S. Myrabo (1997), Discharge and water table predictions using a generalized TOPMODEL formulation, *Hydrol. Processes*, *11*(9), 1145–1167.

Laudon, H., V. Sjoblom, I. Buffam, J. Seibert, and M. Morth (2007), The role of catchment scale and landscape characteristics for runoff generation of boreal streams, *J. Hydrol.*, *344*(3–4), 198–209.

Liu, W., W. Liu, H. Lu, W. Duan, and H. Li (2011), Runoff generation in small catchments under a native rain forest and a rubber plantation in Xishuangbanna, southwestern China, *Water Environ. J.*, *25*(1), 138–147.

Lyon, S. W., S. L. E. Desilets, and P. A. Troch (2008), Characterizing the response of a catchment to an extreme rainfall event using hydrometric and isotopic data, *Water Resour. Res.*, *44*, W06413, doi:10.1029/2007WR006259.

McDonnell, J. J., M. Bonell, M. K. Stewart, and A. J. Pearce (1990), Deuterium variations in storm rainfall-implications for stream hydrograph separation, *Water Resour. Res.*, *26*(3), 455–458.

McDonnell, J. J., et al. (2007), Moving beyond heterogeneity and process complexity: A new vision for watershed hydrology, *Water Resour. Res.*, *43*, W07301, doi:10.1029/2006WR005467.

McGlynn, B. L., J. J. McDonnell, J. Seibert, and C. Kendall (2004), Scale effects on headwater catchment runoff timing, flow sources, and groundwater-streamflow relations, *Water Resour. Res.*, *40*, W07504, doi:10.1029/2003WR002494.

McGuire, K. J., and J. J. McDonnell (2006), A review and evaluation of catchment transit time modeling, *J. Hydrol.*, *330*(3–4), 543–563.

McGuire, K. J., and J. J. McDonnell (2010), Hydrological connectivity of hillslopes and streams: Characteristic time scales and nonlinearities, *Water Resour. Res.*, *46*, W10543, doi:10.1029/2010WR009341.

Moravec, B. G., C. K. Keller, J. L. Smith, R. M. Allen-King, A. J. Goodwin, J. P. Fairley, and P. B. Larson (2010), Oxygen-18 dynamics in precipitation and streamflow in a semi-arid agricultural watershed, Eastern Washington, USA, *Hydrol. Processes*, *24*(4), 446–460.

Mulholland, P. J., G. V. Wilson, and P. M. Jardine (1990), Hydrogeochemical response of a forested watershed to storms—Effects of preferential flow along shallow and deep pathways, *Water Resour. Res.*, *26*(12), 3021–3036, doi:10.1029/WR026i012p03021.

Nash, J., and J. Sutcliffe (1970), River flow forecasting through conceptual models I. A discussion of principles, *J. Hydrol*, *10*, 282–290.

Onda, Y., M. Tsujimura, J. I. Fujihara, and J. Ito (2006), Runoff generation mechanisms in high-relief mountainous watersheds with different underlying geology, *J. Hydrol.*, *331*(3–4), 659–673.

Pionke, H. B., and D. R. Dewalle (1992), Intrastorm and interstorm O-18 trends for selected rainstorms in Pennsylvania, *J. Hydrol.*, *138*(1–2), 131–143.

Pomeroy, J. W., D. M. Gray, T. Brown, N. R. Hedstrom, W. L. Quinton, R. J. Granger, and S. K. Carey (2007), The cold regions hydrological process representation and model: A platform for basing model structure on physical evidence, *Hydrol. Processes*, *21*(19), 2650–2667.

Renshaw, C. E., X. H. Feng, K. J. Sinclair, and R. H. Dums (2003), The use of stream flow routing for direct channel precipitation with isotopically-based hydrograph separations: The role of new water in stormflow generation, *J. Hydrol.*, *273*(1–4), 205–216.

Rinaldo, A., K. J. Beven, E. Bertuzzo, L. Nicotina, J. Davies, A. Fiori, D. Russo, and G. Botter (2011), Catchment travel time distributions and water flow in soils, *Water Resour. Res.*, *47*, W07537, doi:10.1029/2011WR010478.

Roa-Garcia, M. C., and M. Weiler (2010), Integrated response and transit time distributions of watersheds by combining hydrograph separation and long-term transit time modeling, *Hydrol. Earth Syst. Sci.*, *14*(8), 1537–1549.

Salazar, O., A. Joel, I. Wesstrom, H. Linner, and R. W. Skaggs (2010), Modelling discharge from a coastal watershed in southeast Sweden using an integrated framework, *Hydrol. Processes*, *24*(26), 3837–3851.

Seibert, J., and J. J. McDonnell (2002), On the dialog between experimentalist and modeler in catchment hydrology: Use of soft data for multicriteria model calibration, *Water Resour. Res.*, *38*(11), 1241, doi:10.1029/2001WR000978.

Seibert, J., A. Rodhe, and K. Bishop (2003), Simulating interactions between saturated and unsaturated storage in a conceptual runoff model, *Hydrol. Processes*, *17*(2), 379–390.

Shanley, J. B., C. Kendall, T. E. Smith, D. M. Wolock, and J. J. McDonnell (2002), Controls on old and new water contributions to stream flow at some nested catchments in Vermont, USA, *Hydrol. Processes*, *16*(3), 589–609.

Sherman, L. K. (1932), Streamflow from rainfall by the unit graph method, *Eng. News Rec.*, *108*, 501–505.

Sidle, R. C., Y. Tsuboyama, S. Noguchi, I. Hosoda, M. Fujieda, and T. Shimizu (1995), Seasonal hydrologic response at various spatial scales in a small forested catchment, Hitachi-Ohta, Japan, *J. Hydrol.*, *168*(1–4), 227–250.

Sidle, R. C., Y. Tsuboyama, S. Noguchi, I. Hosoda, M. Fujieda, and T. Shimizu (2000), Stormflow generation in steep forested headwaters: A linked hydrogeomorphic paradigm, *Hydrol. Processes*, *14*(3), 369–385.

Sklash, M. G. (1990), Environmental isotope studies of storm and snowmelt runoff generation, in *Process Studies in Hillslope Hydrology.*, edited by M. G. Anderson and T. P. Burt, pp. 410–435, John Wiley and Sons, New York.

Sklash, M. G., and R. N. Farvolden (1979), Role of groundwater in storm runoff, *J. Hydrol.*, *43*(1–4), 45–65.

Son, K., and M. Sivapalan (2007), Improving model structure and reducing parameter uncertainty in conceptual water balance models through the use of auxiliary data, *Water Resour. Res.*, *43*, W01415, doi:10.1029/2006WR005032.

Soulsby, C., and S. M. Dunn (2003), Towards integrating tracer studies in conceptual rainfall-runoff models: Recent insights from a sub-arctic catchment in the Cairngorm Mountains, Scotland, *Hydrol. Processes*, *17*(2), 403–416.

Tetzlaff, D., S. Uhlenbrook, S. Eppert, and C. Soulsby (2008), Does the incorporation of process conceptualization and tracer data improve the structure and performance of a simple rainfall-runoff model in a Scottish mesoscale catchment?, *Hydrol. Processes*, *22*(14), 2461–2474.

Tsuboyama, Y., R. C. Sidle, S. Noguchi, and I. Hosoda (1994), Flow and solute transport through the soil matrix and macropores of a hillslope segment, *Water Resour. Res.*, *30*(4), 879–890.

Uchida, T., and Y. Asano (2010), Spatial variability in the flowpath of hillslope runoff and streamflow in a meso-scale catchment, *Hydrol. Processes*, *24*(16), 2277–2286.

Uchida, T., Y. Asano, T. Mizuyama, and J. J. McDonnell (2004), Role of upslope soil pore pressure on lateral subsurface storm flow dynamics, *Water Resour. Res.*, *40*, W12401, doi:10.1029/2003WR002139.

Uchida, T., I. T. Meerveld, and J. J. McDonnell (2005), The role of lateral pipe flow in hillslope runoff response: an intercomparison of non-linear hillslope response, *J. Hydrol.*, *311*(1–4), 117–133.

Wagener, T., H. S. Wheater, and H. V. Gupta (2004), *Rainfall-Runoff Modeling in Gauged and Ungauged Catchments*, 306 pp., World Sci. Publ., London.

Weiler, M., B. L. McGlynn, K. J. McGuire, and J. J. McDonnell (2003), How does rainfall become runoff? A combined tracer and runoff transfer function approach, *Water Resour. Res.*, *39*(11), 1315, doi:10.1029/2003WR002331.

Wolock, D. M., J. Fan, and G. B. Lawrence (1997), Effects of basin size on low-flow stream chemistry and subsurface contact time in the Neversink River Watershed, New York, *Hydrol. Processes*, *11*(9), 1273–1286.

Wood, E. F., M. Sivapalan, K. Beven, and L. Band (1988), Effects of spatial variability and scale with implications to hydrologic modeling, *J. Hydrol.*, *102*(1–4), 29–47.

Woods, R., M. Sivapalan, and M. Duncan (1995), Investigating the representative elementary area concept—An approach based on field data, *Hydrol. Processes*, *9*(3–4), 291–312.